fibers

Article

Constitutive Model for Plain and Steel-Fibre-Reinforced Lightweight Aggregate Concrete Under Direct Tension and Pull-Out

Hasanain K. Al-Naimi and Ali A. Abbas *

Department of Engineering and Construction, School of Architecture, Computing and Engineering, University of East London, Docklands Campus, London E16 2RD, UK
* Correspondence: abbas@uel.ac.uk

Abstract

In the present study, a programme of experimental investigations was carried out to examine the direct uniaxial tensile (and pull-out) behaviour of plain and fibre-reinforced lightweight aggregate concrete. The lightweight aggregates were recycled from fly ash waste, also known as Pulverised Fuel Ash (PFA), which is a by-product of coal-fired electricity power stations. Steel fibres were used with different aspect ratios and hooked ends with single, double and triple bends corresponding to 3D, 4D and 5D types of DRAMIX steel fibres, respectively. Key parameters such as the concrete compressive strength f_{lck}, fibre volume fraction V_f, number of bends n_b, embedded length L_E and inclination angle θ_f were considered. The fibres were added at volume fractions V_f of 1% and 2% to cover the practical range, and a direct tensile test was carried out using a purpose-built pull-out test developed as part of the present study. Thus, the tensile mechanical properties were established, and a generic constitutive tensile stress–crack width σ-ω model for both plain and fibrous lightweight concrete was created and validated against experimental data from the present study and from previous research found in the literature (including RILEM uniaxial tests) involving different types of lightweight aggregates, concrete strengths and steel fibres. It was concluded that the higher the number of bends n_b and the higher the volume fraction V_f and concrete strength f_{lck}, the stronger the fibre–matrix interfacial bond and thus the more pronounced the enhancement provided by the fibres to the uniaxial tensile residual strength and ductility in the form of work and fracture energy. A fibre optimisation study was also carried out, and design recommendations are provided.

Keywords: lightweight concrete; hooked-end steel fibres; constitutive tensile s-w model; uniaxial tensile behaviour; pull-out behaviour; fracture energy; ultimate bond strength; fibre optimisation

check for updates

Academic Editor: Luciano Ombres

Received: 21 March 2025
Revised: 28 April 2025
Accepted: 12 June 2025
Published: 23 June 2025

Citation: Al-Naimi, H.K.; Abbas, A.A. Constitutive Model for Plain and Steel-Fibre-Reinforced Lightweight Aggregate Concrete Under Direct Tension and Pull-Out. *Fibers* **2025**, *13*, 84. https://doi.org/10.3390/fib13070084

1. Background Review

1.1. Lightweight Aggregate Concrete

Recently, there has been a rapid growth in concrete technology that is particularly directed towards sustainability and upgrading the strength-to-weight ratio [1]. Achieving the latter results in a reduction in the building mass, which leads to savings in materials, construction time and—crucially—a reduction in costs and adverse effects of carbon emissions (including in the transportation of fewer materials). Therefore, the use of structural lightweight aggregate concrete (LWAC) as a replacement to the conventional heavier normal weight concrete (NWC) counterpart helps achieve such goals. In addition, the lightweight aggregate used in this work is made from recycled waste and thus offers the advantage of a further reduction in CO_2 emissions, and it is an alternative to depleting quarried natural resources [2]. Recycled aggregates are made from fly ash waste (commonly known as LYTAG), which is a by-product of coal-fired electricity power stations [3]. Fly ash, also termed Pulverised Fuel Ash (PFA), is ash resulting from the burning of pulverised coal in these power stations. Several studies support the environmental benefits provided by this PFA-based material and its effectiveness in reducing carbon emissions [4]. Additionally, it should be noted that LWAC brings other advantages such as increased thermal insulation, noise absorption and fire resistance [5,6]. Thus, the use of lightweight concrete can allow for taller and longer span structures and is also beneficial in situations when a reduction in inertial loads is needed, such as in seismic zones [7–10]. Nonetheless, despite these benefits, some disadvantages have been highlighted with the use of LWAC. One of the key shortcomings is the increased brittleness of lightweight concrete in comparison to its normal weight counterpart, which is likely due to the porous concrete matrix and its poor aggregate interlock mechanism. This leads to a complete absence of the strain softening mechanism post-cracking [2]. Therefore, for plain LWAC, instantaneous failure is observed both in compression and tension at the *material* level once peak stress is reached. Similarly, a drastic reduction in shear capacity, excessive deflection and cracking due to the lower modulus of elasticity is expected at the *structural* level [11–14]. Despite the fact that modern structural LWAC has been available for over several decades, its mechanical properties have not been comprehensively researched, and the material and structural equations defining its behaviour have been traditionally adapted from dated studies on NWC [12,14–18].

1.2. Steel Fibres

To address the increased brittleness of LWAC, steel fibre reinforcement has emerged as a potential solution whose effectiveness has been proven in increasing the ductility of other fibrous composites in the past [19–23]. This is because one of the key benefits to steel fibres is enhancement to ductility. Their key advantage over conventional bar reinforcement is the reduction in construction time as they can conveniently be added to the concrete ready mix delivered, hence leading to economic and environmental benefits. Steel-fibre-reinforced concrete (SFRC) is also particularly useful for smaller cross-sectional elements and for sprayed concrete, e.g., shotcrete, which is commonly used in tunnel lining. Another potential method is to relax the shear reinforcement spacing at beam ends [24] and in critical elements in seismic-resistant design, such as beam-column joints [21], which can get congested with conventional bar reinforcement, leading to practical construction difficulties. Hooked-end steel fibres are the most commonly used type and are usually made by cutting steel wire into short lengths and then cold-drawing them to create a hook shape at one end. This type of steel fibre is mainly used in structural applications due to its improved bond properties with concrete (compared to straight fibres without end hooks). The bond can be further enhanced by increasing the number of end hooks. The present study examines the performance of single and multiple end hook arrangements. Straight steel fibres, on the other hand, have a smooth surface that reduces friction (and bond with concrete as a consequence). They are usually used in thin concrete structures such as precast concrete panels and overlays, and in applications with less demanding structural performance.

Although somewhat limited, research studies on fibrous lightweight concrete have been reported for several years [25]. However, at present, there are hardly any international standards specific to steel-fibre-reinforced lightweight concrete (SFRLC), with current guidelines usually being adapted from fibrous normal weight concrete (SFRC). The practical application of steel fibre reinforcement in lightweight concrete is still in its infancy, and it is largely carried out at the *structural* level only in the form of case studies that largely involve lightweight aggregates (such as pumice stone and oil palm aggregates) different to the ones investigated in the present research work [22,23,26–28]. The recycled PFA-based aggregates used in this study are well established for structural use by the construction industry, so they represent a good benchmark to test the addition of fibres, meaning that the ensuing findings and recommendations will be useful to current practice. It should also be borne in mind that coal-fired power generation remains the largest contributor of energy in the world [29]; even with the decommissioning of coal plants, there is still a large amount of historical waste. Therefore, the present comprehensive study on fibrous recycled PFA-based lightweight aggregate concrete is particularly beneficial in providing sustainable design solutions for the rapidly developing fibrous concrete technology. The present study is part of a large experimental programme which examined the structural behaviour of steel-fibre-reinforced recycled PFA-based lightweight concrete at both the *material* and *structural* levels [30]. The compression structural responses of SFRLC were examined in an earlier publication [31]. The present article is focused on the series of tests that were carried out to investigate the uniaxial tensile and pull-out behaviour of lightweight concrete reinforced with different hooked-end steel fibres at fibre volume fractions V_f of 1% and 2%.

1.3. Tensile Behaviour and Limitations of Existing Research

Under tensile loading, as the principal tensile stress applied exceeds the ultimate tensile resistance of plain concrete, microcracks start to form and morph into a single larger macrocrack, which eventually leads to concrete failing in tension, thus releasing the stored energy of the system [32]. When fibres are added, a crack-arresting action takes place once cracks have formed, and then fibres create a bridge between the ends of the crack to resist its extension. However, as the principal tensile stress grows, and due to sliding friction, the fibres may end up being pulled out or ruptured depending on the number of fibres crossing the crack (which, provided that a good mixing process is used, usually correlates with the fibre volume fraction V_f) and the fibre-matrix interfacial bond strength. The latter is largely governed by the geometry of fibre, its tensile strength, mechanical anchorage, embedment length, inclination angle and concrete strength. These factors govern the post-crack behaviour of fibrous concrete. Researchers such as Löfgren [33] and Lee et al. [34] detailed this behaviour for fibrous normal weight concrete, which benefits from the combined effect of fibre reinforcement and the residual effect of aggregate interlock mechanism once crack develops. Given that the aggregate interlock mechanism is expected to be negligible for lightweight concrete, this effect might be different for fibrous lightweight concrete in the post-cracking phase.

Indirect tensile tests to investigate the flexural tensile behaviour of fibrous concrete can be found in the literature [7,19,26,35–38]. It is established that the addition of steel fibres upgrades the flexural behaviour of lightweight concrete. However, the uniaxial tensile behaviour of fibrous lightweight concrete has not been thoroughly investigated to establish analytical models. This important aspect is addressed in the present research work because, unlike flexural testing, direct uniaxial tensile testing offers the ideal results required to understand the tensile pre- and post-cracking behaviour of concrete and the interaction of LWAC with fibres. Currently, limited comprehensive studies were found in the literature that are focused on the investigation of the uniaxial tensile stress–strain (σ-ε) or stress–crack width (σ-ω) behaviour and pull-out behaviour of SFRLC. Amongst all the available research examined, it seems that only Grabois et al. [23] and Mo et al. [39] carried out direct uniaxial tensile tests on lightweight concrete using the dog bone test [40] and the RILEM TC 162-TDF uniaxial test [41], respectively. They reported an increase in uniaxial tensile residual strength with hooked-end steel fibre reinforcement with $V_f \leq 0.5\%$ and $V_f < 1\%$ compared to plain LWAC, respectively. Grabois et al. [23] showed a stress–strain relationship, while Mo et al. [39] only estimated the tensile strength. Moreover, there seems to be a lack of thorough investigations on the pull-out tensile behaviour of fibrous PFA-based lightweight aggregate concrete, especially with modern multi-bend fibres like the ones used in the present study.

Therefore, the present research work aims to offer more clarity on and a greater understanding of the uniaxial tensile and pull-out behaviour of steel-fibre-reinforced lightweight concrete and presents valuable additional experimental data to enrich the current available literature. This study involved determining the tensile properties, including tensile σ-ω constitutive models for SFRLC, the fracture energy G_f and bond strength. It also led to the development of a fibre optimisation study based on different hooked-end steel fibre types, geometries and contents and different compressive strengths of plain lightweight concrete.

2. Experimental Procedure

The mixing process, materials, grading, vibration, curing and specimen preparation process were all detailed in a preceding paper, which was focused on the compression behaviour of SFRLC [31] as part of a comprehensive experimental research programme [30]. For the sake of completeness and to avoid repetition, only new data are presented in this study.

2.1. Material Properties

The chemical and geometrical properties of cement, natural sand and PFA-based coarse aggregates used in the experiments are detailed elsewhere [30,31].

Recycled sintered pulverised fly ash aggregates were used as the coarse aggregates for the lightweight concrete in the present experimental study. Fly ash is a by-product of coal-fired electricity power stations [3]. The aggregates (4–14 mm) are brown, roughly spherical with a honeycomb structure of interconnected voids. They have a specific gravity of about 1.8 and a water absorption capacity of up to 15%. Natural sharp sand with a maximum aggregate size of 4.75 mm was used as the fine aggregate of the concrete. In the present study, Dramix hooked-end (single-bend) 3D fibres with different aspect ratios were incorporated as reinforcement for the pull-out specimens. The fibres tested in this work are shown in Figure 1, while their geometrical properties, which were adapted from Abdallah et al. [42,43], are shown in Table 1. A schematic representation of the parameters shown in Table 1 is depicted in Figure 2. It should be noted that hooked-end 3D fibres were regarded as the control fibres during the experimental programme. The rest of the fibres were used in order to evaluate the effects of different fibre geometries, bends, lengths and diameters on the behaviour of lightweight concrete.

Table 1. Properties of hooked-end fibres used [44]. Geometrical properties of hooks are adapted from [42,43].

Fibre Type	σ_u (MPa)	e_u (%)	*E* (GPa)	σ_y (MPa)	L_f (mm)	d_f (mm)	L1 (mm)	L2 (mm)	L3 (mm)	L4 (mm)	θ_1 (°)	θ_2 (°)	β (°)
3D	1160	0.8	210	775–985	60	0.9	2.12	2.95	-	-	45.7	-	67.5
3D*	1225	0.8	210	775–985	60	0.75	-	-	-	-	-	-	-
3D**	1345	0.8	210	775–985	35	0.55	2.55	2.22	-	-	38.3	-	70.9
4D	1500	0.8	210	1020–1166	60	0.9	2.98	2.62	3.05	-	30.1	30.8	75
5D	2300	6	210	1177–1455	60	0.9	2.57	2.38	2.57	2.56	27.9	28.2	76

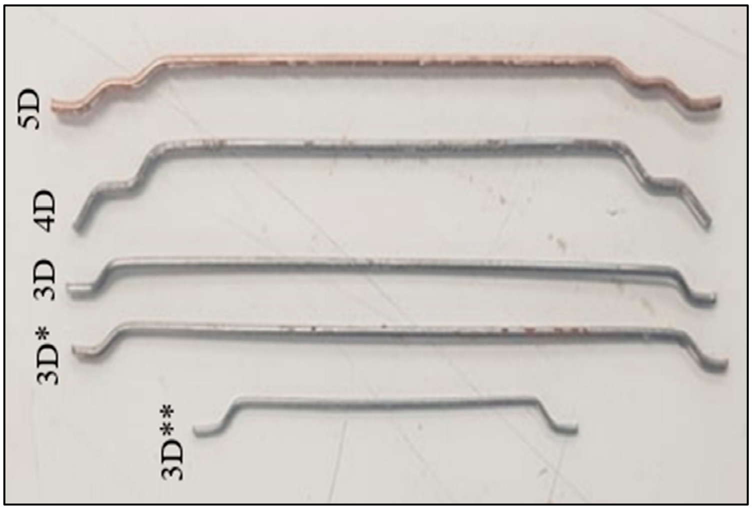

Figure 1. Fibres used in this work.

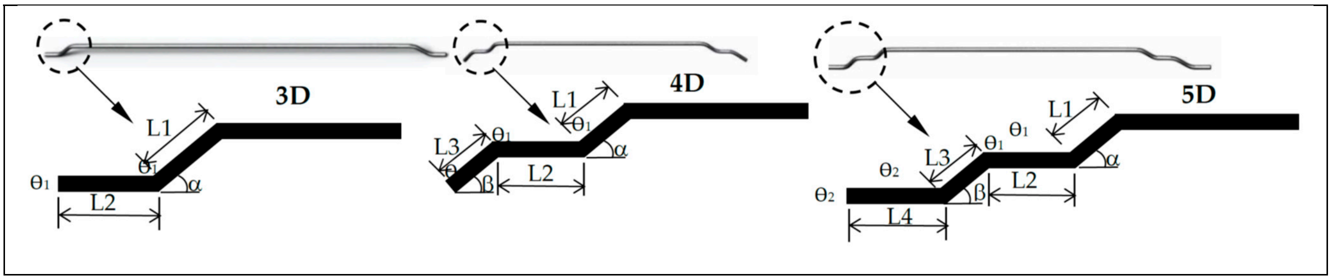

Figure 2. Schematic representation of parameters shown in Table 1 (adapted from [42]).

2.2. Properties of Mixes

In addition to the 4 mixes cast in the preceding study on compressive behaviour [30,31], mixes 1-3D* and 1-3D** were added with fibres 3D* and 3D**, respectively (as summarised in Table 2).

Table 2. Mix design.

Mix	V_f (%)	Fibre	$f_{lck}/f_{lck,cube}$	Cement (kg/m^3)	Sand (kg/m^3)	PFA-Based Aggregates (kg/m^3)	Effective Water (kg/m^3)
1-3D	1–2 (80–160 kg/m^3)	3D	LC30/33	370	592	635.6	175
1-3D*		3D*					
1-3D**		3D**					
1-4D		4D					
2		3D	LC35/38	420	546		
3		5D	LC40/44	480	485		

2.3. Test Method for Pull-Out Test

In this section, the details of the design and method of uniaxial tensile pull-out tests on notched prisms are provided. Uniaxial compression cube and cylinder tests with their setups and instrumentations are detailed in an accompanying paper [30,31]. For the pull-out tests, each mix included two repeated notched prism specimens per volume fraction V_f dosage. Building on the previous experimental study by Robins et al. [45], a direct uniaxial tensile pull-out test was designed in the present study, which can be used for both plain and fibrous concrete. The aim was to investigate the effect of the embedded fibres on the uniaxial tensile stress–crack width response of lightweight concrete. The main difference between the test setup proposed in this study and the one by Robins et al. [45] is that for the latter, the steel fibre is embedded in concrete on one end and in a high strength mortar on the other end to grip the fibres and practically prevent their movement on that side, while the fibre in the test setup proposed in this study is embedded in the lightweight concrete matrix on both ends. Hence, Robins et al.'s test [45] is practically similar to the conventional single fibre pull-out test shown in other studies [42,46–48].

The designed uniaxial tensile pull-out test adopted in this work (depicted in Figure 3) carries several advantages. First, it provides, to a large extent, a truer representation of the behaviour of steel fibres bridging a crack in a real structural element as compared to the classic pull-out tests explained earlier since fibres are completely embedded in lightweight concrete, while the crack is not predefined but induced by a reduced section (notch) spanning 10 mm in the middle of the specimen. The reason for designing this notch is to allow the continuity of lightweight concrete constituents of the specimen (sand, PFA-based aggregates and cement) through the notch at which breakage is ensured. Also, the notch allows for the introduction of the embedment length L_E as a variable and enables the specimen to be monitored in the middle section in terms of load–slip behaviour. Since the crack is not predefined, it was possible to derive the peak tensile cracking load of LWAC and SFRLC when their behaviour was elastic. Secondly, by taking into consideration V_f in the effective area of the cylinder around the embedded fibre, this test can be regarded as both a fibre pull-out test and a uniaxial tensile test. Similarly to the previous experimental study by Robins et al. [45], the effective area of the notched cylinder through which the fibre is embedded was determined using numerical and statistical models, which depend mainly on fibre geometry and fibre volume fraction [49–51]. Therefore, the diameter of the notch was calculated to be 12 mm and corresponds to V_f = 1% for DRAMIX hooked-end fibres of d_f = 0.9 mm (3D, 4D and 5D). It should be noted that to test the concrete for V_f = 2%, simply another fibre was added. The fibre spacing was equal in the notch.

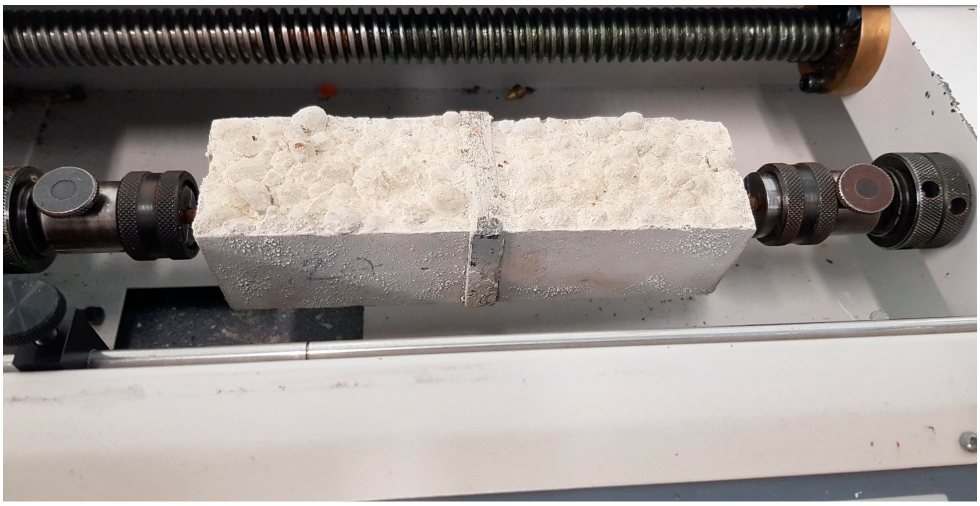

Figure 3. Proposed notched prism being tested in the direct uniaxial tensile pull-out machine.

Based on the concrete fibre–matrix interfacial properties which are directly affected by the densification of the matrix and the water/cement (w/c) ratio of concrete (which influence the compressive strength), fibre content V_f, aspect ratio a_f, mechanical anchorage (number of bends or hooks), embedment length L_E, orientation angle, dispersion and tensile strength [45,48,52,53], the stress–crack width relationship was derived. The aforementioned factors govern the bond-slip behaviour between concrete and fibres, which in turn influences the tensile behaviour both at the *material* and *structural* levels of SFRLC. Hence, the evaluation of the results of this test explicitly enables the prediction of the behaviour of SFRLC members, such as beams and slabs. It should be noted that 2 moulds with different dimensions were designed to test 2 different types of pull-out notched prism specimens for each mix (shown in Figure 4). The pull-out notched prism specimens were produced using both moulds A and B.

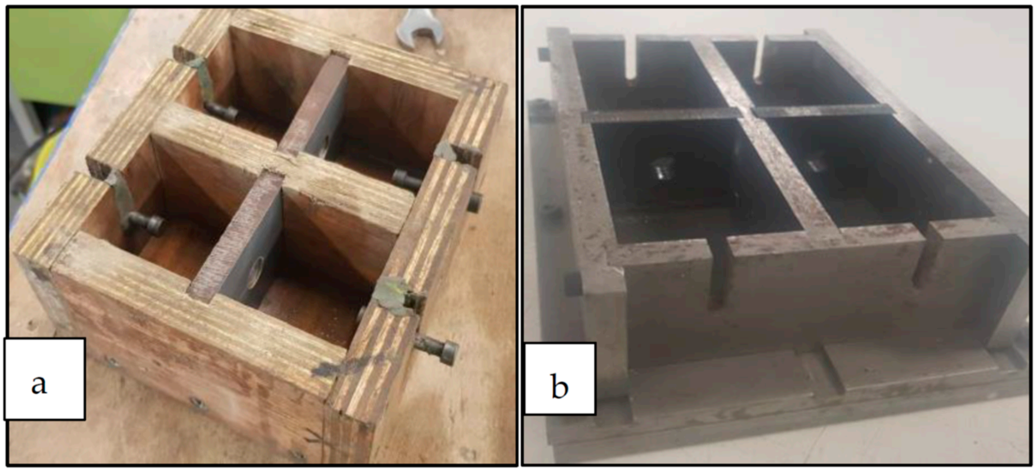

Figure 4. Mould A (**a**) and mould B (**b**).

Each mould contained 2 identical chambers. The differences in dimensions between moulds A and B are shown in Figure 5. The reason behind testing 2 different types of notched prisms in the pull-out test was to ensure the development of an accurate and realistic stress–crack width relationship of fibrous lightweight concrete independent of the size effects of the specimen used, and thus, it can be applied to any structural member. Preliminary trials showed that both moulds yielded similar results for identical specimens in terms of the pull-out load–slip behaviour and failure patterns. Therefore, the stress–crack width relationship derived based on these tests can be applied directly to FE models unlike the more common stress–strain relationship, which usually requires calibration or the study of the structural characteristic length l_{cs}, which is used to derive strain ε with $\varepsilon = \omega/l_{cs}$. To prepare the pull-out specimen before casting, the fibre was positioned at the notch for the chosen L_E and the required inclination angle to the load, using fixed fine suspended cables mechanically attached to the fibre. These were removed once concrete was cast to avoid any potential interference with the results.

During the pull-out test photographed in Figure 3, as the 2 short rigid carbon steel bars (embedded at the ends of the specimen) were being pulled in opposite directions using machine grips, the cylindrical concrete volume through which the fibre was embedded became subjected to pure unidirectional tension. The embedded carbon steel bars had enlarged ends and were further prevented from potential slip with steel washers attached to their heads. Although possible slip of small steel bars might occur before concrete cracking, both concrete blocks embedding the two hooked ends of the fibre were assumed to be rigid following concrete cracking. Since the bond of the carbon steel bar with the lightweight concrete matrix is higher than that of hooked-end steel fibres, the pull-out response of the fibrous lightweight concrete specimen was designed to only occur along the fibre and the surrounding concrete. These assumptions were found to be correct, as shown in the Results Section. The tensile machine was calibrated and fitted with a sensitive displacement transducer capable of accurately measuring the slip once the crack was initiated. The pull-out specimen was carefully placed in the tensile testing machine with a maximum load cell capacity of 20 kN, where the two carbon steel bars from each end were securely gripped in a way to disallow any superfluous slip. While one end was fixed, the other end was gradually pulled in tension at a displacement-controlled loading rate of 1 mm/min with 2 readings recorded every 1 s.

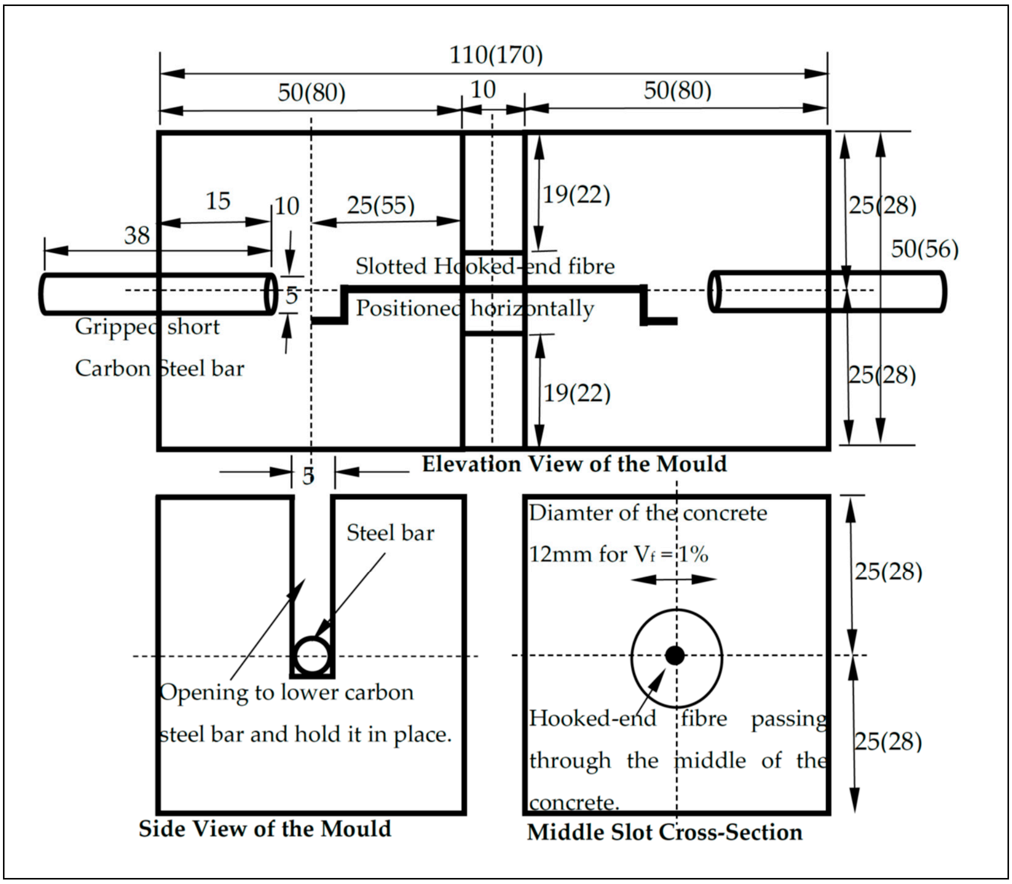

Figure 5. Dimensions of 1 chamber in pull-out moulds A and B. Values between brackets are for mould B dimensions only. All dimensions are in mm.

Cao and Yu [54] found that the embedment length plays a dominant role in the behaviour of fibre pull-out as a short embedment length at an inclination angle of 30° degrees for ultra-high-performance concrete caused matrix fracture failure. Robins et al. [45] also suggested that unless the embedment length is higher than the hooked-end length, the pull-out load is reduced. Abdallah et al. [48] concluded that the embedment length had no influence on the pull-out strength but merely increased the slip and ductility. Hence, it is important to investigate the effect of L_E on SFRLC. For instance, although a 30 mm embedment length maximises the frictional fibre pull-out for 3D fibres used (d_f = 60 mm), it is thought that an embedment length L_E = 30 mm can lead to an unrealistically favourable case of uniaxial tensile tests, as in the cracking of a real structural member can manifest anywhere along the fibre and is more likely to occur at a shorter embedment length. Thus, the embedment length was initially fixed at 30 mm, 20 mm and 10 mm for different specimens based on a crack that is expected to take place in the middle of the 10 mm notch.

An angle of 0° to the load is considered as the most unfavourable in a hooked-end fibre pull-out test due to the lowest possible frictional resistance and the shortest required length for fibre straightening (only hooks will be straightened) before being pulled out. Consequently, the fibre stress developed during pull-out will be lower than the maximum stress capacity of the fibre. If the angle is too large, concrete matrix fracture failure could also develop due to matrix spalling caused by the snubbing effect along the bent part of the steel fibre [54]. Depending on the fibre tensile strength, in theory, as the angle to the load is increased, frictional resistance is increased, which results in an increase in the uniaxial tensile strength of SFRLC until the maximum tensile strength of the fibre is reached, leading to rupture, so long as the concrete matrix does not break due to the concentrated normal force from the fibre and given that the embedment length does not reduce to the point where the hook is not well bonded. Recent research on ultra-high-strength concrete conducted by Cao and Yu [54] revealed that the inclination angle for the maximum pull-out load can be around 20–30° to the horizontal (and 10–20° for Robins et al. [45]) provided that the fibre tensile strength is high enough to prevent fibre rupture and the matrix is strong and dense enough to prevent matrix fracture. Since the lightweight concrete used is not as dense as ultra-high-strength or normal weight concrete, since LWAC is known to have air pores, and for design purposes [55], it was decided that an angle of 0° was to be adopted as the base for design in the pull-out tests, while a few specimens with other angles were tested for completeness.

Finally, the aspect ratio which is defined as L_f/d_f can also impact the pull-out behaviour. It was found that the longer the fibre, the more efficient the crack bridging [42]. Based on all of the above observations, the testing programme comprised an extensive fibre pull-out investigation which considered the following parameters: V_f = 0, 1 and 2%; f_{lck} = 30, 35 and 40 MPa; L_f/d_f = 65 and 80; d_f = 0.55, 0.75 and 0.9 mm; L_f = 35 and 60 mm; number of fibre hooks or bends n_b = 1(3D), 2(4D) and 3(5D); and inclination angles of 20° and 45°. Also, 3D and 5D fibres with the hooks cut off were tested to check the viability of mixing straight fibres of different tensile strengths with lightweight concrete and to quantify the contribution of the hooks on the pull-out behaviour.

3. Results and Discussion

The workability, density and uniaxial compressive cube strength results were detailed in an accompanying paper for mixes 1-3D, 1-4D, 2 and 3 [30,31]. The additional mixes 1-3D* and 1-3D** showed similar workability, density properties and compressive strength results to mix 1-3D, and these results are summarised in Table 3 (data for convenience mixes 1–3 are also included). To avoid repetition, the interpretation of the results and trends can be directly adopted from accompanying studies [30,31]. In summary, it was found that the mechanical properties were improved with the addition of fibres, and the density was largely unaffected, which is important for LWAC applications. On the other hand, the workability was significantly reduced with the addition of more than a 2% volume fraction of fibres. This further emphasises that for fibrous mixes, the fibre dosage should not exceed V_f = 1.5–2% based on workability challenges if no superplasticisers or water-reducing agents are used. It also appears that the mixes having fibres with more extensive hooks held the slump together more tightly, which led to lower slump values than the mixes having fibres with less extensive hooks. It should be noted that mix 1-3D** with the shortest fibres 3D** exhibited the highest slumps and highest densities amongst all mixes.

Table 3. Mean values of slump, water-saturated density (oven-dry density with *) and average cube compressive strength for mixes 1–3. Standard deviation is shown between brackets.

Mix	f_{lck} (MPa)	Fibre	Slump (mm)			Density (kg/m^3)			$f_{lcm,cube}$ (MPa)		
			Plain	V_f = 1%	V_f = 2%	Plain	V_f = 1%	V_f = 2%	Plain	V_f = 1%	V_f = 2%
1-3D	30	3D	91 (7.6)	66 (3.1)	32 (5.2)	1981 (124) *1723 (159)	1992 (182)	1979 (133)	37 (3.1)	37 (4.1)	38 (3.2)
1-3D*	30	3D*	96 (8.1)	57 (3.1)	31 (2.8)	1968 (144) *1693 (163)	1963 (161)	1979 (189)	39 (2.2)	41 (3.8)	40 (3.1)
1-3D**	30	3D**	103 (10.2)	87 (4.4)	42 (4.6)	2001 (137) *1731 (122)	1991 (149)	1986 (173)	37 (5.1)	38 (2.9)	37 (6.3)

Table 3. *Cont.*

Mix	f_{lck} (MPa)	Fibre	Slump (mm)			Density (kg/m^3)			$f_{lcm,cube}$ (MPa)		
			Plain	V_f = 1%	V_f = 2%	Plain	V_f = 1%	V_f = 2%	Plain	V_f = 1%	V_f = 2%
1-4D	30	4D	98 (11.2)	49 (3.3)	26 (4.1)	1998 (166) *1777 (172)	1962 (171)	1951 (111)	36 (4.3)	37 (3.8)	34 (4.2)
2	35	3D	86 (7.2)	46 (6.1)	28 (2.1)	2000 (178) *1786 (153)	1988 (182)	1963 (121)	45 (5.6)	42 (3.8)	44 (3.2)
3	40	5D	88 (4.9)	42 (1.3)	20 (2.6)	1954 (121) *1712 (142)	1936 (168)	1917 (167)	50 (6.8)	49 (4.2)	51 (3.1)

3.1. Pull-Out Load–Slip Behaviour

A fully straightened hooked-end 3D fibre photographed at the end of testing is shown in Figure 6. It can be seen that the effective cylinder through which the fibre was embedded contained aggregates as well as cement and sand at the notch through which the fibre was centred. This proves that the mould used and the testing design adopted were adequate at mimicking the realistic behaviour of SFRLC at the crack.

Figure 6. The pull-out specimen at the end of testing.

Figure 7 depicts the pull-out load–slip behaviour of some key specimens tested (with the salient features summarised in Table 4). Overall, the behaviour of the SFRLC specimens in the pull-out test can be summarised in the following stages: Initially, an elastic stage takes place until the point of cracking. This point approximately coincides with the load at which *plain* concrete would fail in uniaxial tension and is roughly the case for all the specimens of similar concrete grade tested regardless of the type of fibre or fibre volume fraction. This shows that fibres have an insignificant effect on the elastic uniaxial tensile behaviour of SFRLC and only become active once the concrete cracks. In the absence of any innate tension stiffening mechanism, such as in the case of brittle plain lightweight concrete, a sudden drop in load to 0 is seen (which is the case for the plain concrete specimen, i.e., V_f = 0%, shown in Figure 7).

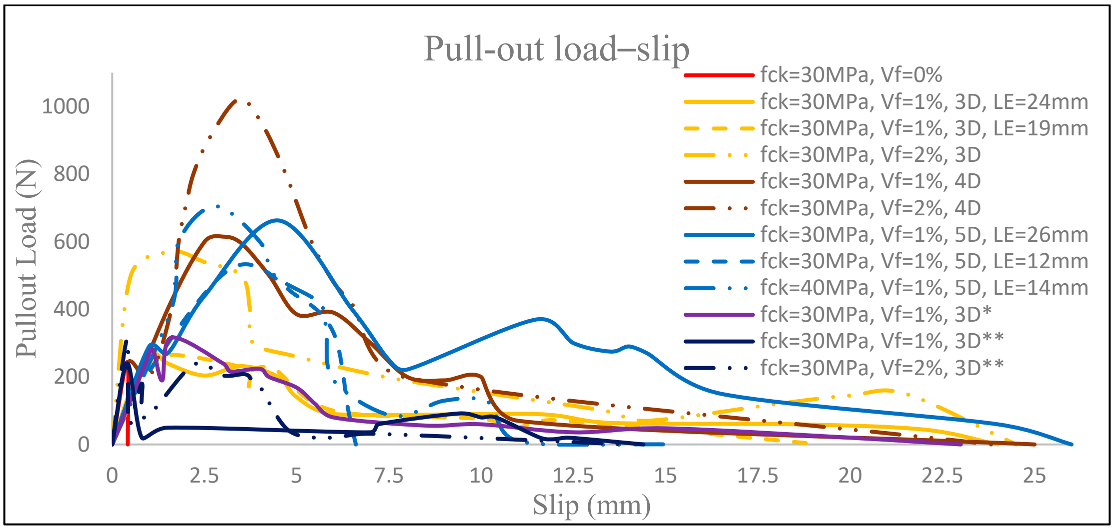

Figure 7. Mean pull-out load–slip behaviour of key specimens tested.

Table 4. Average deformation histories of uniaxial tensile pull-out test. [1] Fibre at angle of 20°; [2] fibre at angle of 45°; [3] fractured concrete; [4] hook-less 5D fibre; [5] hook-less 3D fibre; [6] slip at maximum pullout; [7] ultimate slip where fibre has been pulled out.

f_{lcm} (MPa)	V_f (%)	Fibre Type	L_E (mm)	P_{max} (N)	Δ_{max} [6] (mm)	Contribution of Fibre [Interval] (mm)		Δ_u [7] (mm)
						Hook	Pull-Out	
30.1	0			244	0.8			0.8
36.5	0			267	0.73			0.73
44.1	0			320	0.68			0.68
33.3	1	3D	18.41	265	1.6	[1, 6]	[6, 19.2]	19.2
32.8	1	3D	23.5	266	1.2	[0.6, 6.6]	[6.6, 24]	24
35.0	2	3D	24	570	1.6			24.5
34.9	1	4D	24.4	615	3.1	[0.6, 9.3]	[9.3, 25]	25
34.6	2	4D	23.4	1020	3.4			23.8
34.3	1	4D [1]	18.7	625	6	[0.42, 9.2]	[9.2, 19.1]	19.1
34.1	1	4D [2]	19	690	8.1	[1.1, 8.1]		8.1
36.2	1	3D	12.9	326	1.8	[1.4, 6.4]	[6.4, 13.9]	13.9
34.6	1	5D	25	662	4.5	[2.5, 12.5]	[12.5, 26]	26
44.1	1	5D	14.45	705	2.8	[1.1, 11.1]	[11.1, 15.1]	15
44.1	1	5D [3]	11	520	3.2	[1, 5]		12
31.5	0.7	3D*	21.7	316	1.6	[1.35, 6.3]	[6.3, 23]	23
31.0	0.4	3D**	14	92	9.4	[7.2, 12.4]	[12.4, 14.4]	14.4
38.2	1.2	3D**	13.6	236	2.2			14
32.4	1	5D [4]	14.8	30–56	1.2		[0.4, 15.2]	15.2
32.4	1	3D [5]	20.8	34–52	0.42		[0.4, 23]	21.4

With the incorporation of steel fibres, however, the plain lightweight concrete peak tensile strength where the principal crack is fully formed is followed by a drop and then an increase in load. This behaviour largely agrees with that observed in the uniaxial tensile tests on SFRC carried out by Barragán et al. [56] and Abdallah et al. [42] and the pull-out tests performed by Robins et al. [45]. This marks the fibre bridging phase, which is initially characterised by an elastic behaviour followed by fibre debonding where a gradual loss of the frictional bond between the fibre and matrix is seen. Afterwards, the activation of mechanical hooking is initiated. This behaviour was also reported by Qi et al. [55]. This results in an increase in the peak residual tensile load due to fibre reinforcement only. This load is mainly affected by concrete strength, fibre mechanical anchorage (number of hooks), fibre diameter, fibre tensile strength and inclination angle. Also, if the embedment length is not adequate to cater for hook straightening and thus the mobilisation of the maximum possible fibre stress for the composite, the peak load can be drastically reduced due to the possibility of matrix cracking at hook ends. Maintaining this load solely relies on the bond between the steel fibres and concrete. During this stage, the fibre undergoes plastic deformation at hooks, and plastic hinges are developed. The maximum number of plastic hinges at the maximum load become active (two for 3D, three for 4D and four for 5D). This stage is followed by stress relaxation, which is characterised by full hook straightening and the deactivation of the plastic hinges. Finally, frictional fibre–matrix pull-out occurs, and the test ends with the fibre being completely pulled out.

3.1.1. Effect of Number of Bends n_b

To investigate the effect of the number of fibre bends or hooks, specimens with 3D, 4D and 5D fibres with V_f = 1% were all compared. All fibres had an embedded length of approximately L_E = 25 mm (which was established before the test), an identical aspect ratio (L_f/d_f = 65) and similar compressive strengths. A maximum pull-out strength of P_{max} = 267 N was recorded for the 3D sample, while P_{max} = 615 N and P_{max} = 662 N were recorded for both the 4D and 5D samples, respectively. Although not only the number of bends differed between the three fibres but also the maximum fibre tensile strength, the 3D and 4D samples failed after the complete straightening of bends, while the 5D samples showed a partial straightening of bends, and then all fibres were pulled out without fibre rupture taking place. This suggests that the number of bends or hooks is the most influential factor in the behaviour of fibrous lightweight concrete (with the same fibre aspect ratio) and shows that a higher number of bends or hooks may lead to higher pull-out strength since more plastic hinges are developed and more bend straightening is required due to a better concrete–fibre bond being developed. Also, it can be observed that the post-cracking ductility increases with the increase in the number of bends as the load can be maintained at a high stress level for a longer duration of the test. It should be noted, however, that most 5D hooks appeared to not be completely straightened after pull-out (Figure 8). The reasons behind the partial hook straightening of the 5D fibre will be further investigated in Section 3.3.

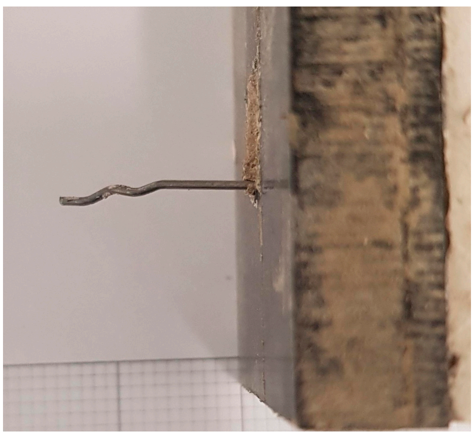

Figure 8. The 5D hook not being fully straightened following the pull-out test.

3.1.2. Effect of Fibre Aspect Ratio a_f

To investigate the effect of the fibre aspect ratio a_f (defined as L_f/d_f), the 3D* fibre with a_f = 80 (L_f = 60 mm, d_f = 0.75 mm) was tested. The 3D* fibre had nearly identical properties, including the maximum fibre tensile strength, length and geometrical hooks to those of the control 3D fibre with a_f = 65 (L_f = 60 mm, d_f = 0.9 mm). However, the 3D* fibre developed a maximum pull-out strength of P = 316 N, which is 15% higher than that of the control 3D fibre. This shows that a higher aspect ratio leads to the development of a higher tensile strength.

3.1.3. Effect of Fibre Length L_f

To study the effect of the fibre length, the 3D** fibre with aspect ratio a_f = 65 (L_f = 35 mm, d_f = 0.55 mm) was tested. The 3D** fibre has an almost identical hook length to the 3D fibre and a slightly higher maximum fibre tensile strength. This fibre proved to be somewhat the weakest as it generated a pull-out force of only P = 92 N. Hence, the longer the fibre, the more efficient the crack arresting mechanism. This agrees well with Abdallah et al.'s [42] findings.

3.1.4. Effect of Fibre Dosage V_f

To study the effect of increasing the fibre dosage, mixes of similar fibre types are compared for different fibre volume fractions (V_f = 1% and 2%). For 3D fibres, the pull-out strength was recorded to be P = 570 N at V_f = 2%, which is 53% higher than the corresponding pull-out strength at V_f = 1%. However, for 4D and 5D fibres, the increases in strength (when V_f was raised from 1% to 2%) were calculated to be 44% and 50%, respectively. This enhancement was expected since the fibre dosage was doubled.

3.1.5. Effect of Compressive Strength f_{lck}

To examine the effect of lowering the concrete grade, specimens with compressive strength f_{lck} = 40 MPa reinforced with 5D fibres were tested. When their pull-out behaviour was compared to that of concrete specimens with f_{lck} = 30 MPa (also reinforced with 5D fibres), the pull-out tensile strength developed was 7% higher for the higher concrete grade. Hence, increasing the concrete grade by increasing the cement content and reducing the w/c ratio leads to a reduction in air pores around the embedded hooks, which increases the mechanical bond strength. This behaviour was also reported by Abdallah et al. [48].

3.1.6. Effect of Embedded Length L_E

To examine the effect of varying the embedment length L_E on the tensile strength, mixes sharing the same properties (f_{lck} = 30 MPa, V_f = 1%, 3D) but with different embedded lengths ($L_{E,1}$ = 18.4 mm and $L_{E,2}$ = 23.5 mm) were compared. For both specimens, a similar pull-out load ($P_{max} \approx 265$ N) was measured, albeit the specimen with a higher embedded length provided higher ductility. The latter will be inspected by calculating the pull-out work performed in Section 3.2.2. It is interesting to observe that some specimens experienced concrete fracture and then pull-out at the hook's location, such as the specimen with the following properties: f_{lck} = 30 MPa, V_f = 1% and 5D fibre. Figure 9 shows a concrete specimen fracturing outside the notch. For this particular sample, the embedded length was only 12 mm, while the hook length is approximately 10.1 mm for 5D fibres. Therefore, the embedment length L_E was deemed insufficient. Another identical specimen with L_E = 14.45 mm was seen to be capable of undergoing complete hook straightening before being pulled out. Therefore, altering the embedment length of the hooked-end fibres for lightweight concrete has no practical effect on the maximum pull-out strength but merely increases the ductility via frictional pull-out as long as L_E provides enough hook bond (i.e., when $L_E \sim L_h + 4.5$ mm with L_h being the hook length). This phenomenon was also observed with 3D and 4D fibres. Hence, if the fibre diameter d_f is to be factored into the previous equation, then $L_E = L_e \sim L_h + 5d_f$, with L_e being the length required to develop the maximum pull-out strength of the fibre based on pull-out tests. This finding also agrees with Abdallah et al.'s [48] observations, who recommended $L_E = L_h + 5$ mm to obtain the maximum pull-out load, P_{max}.

Figure 9. Concrete fracture outside the notch.

3.1.7. Effect of Fibre Inclination Angle θ_f

To study the effect of the orientation angle, which is the angle between the tensile load applied and the fibre, 4D fibres at angles 20° and 45° were tested and plotted (Figure 10). It can be seen that the specimen whose fibre was oriented at 45° failed in concrete fracture similar to the specimens with an inadequate embedded length, although it developed a higher pull-out tensile strength (P = 690 N) than its counterparts. By contrast, a pull-out strength of only P = 626 N was recorded for the specimen with an orientation angle of 20°. However, the latter failed in ductile fibre pull-out mode. This pull-out strength is 11 N higher than that developed by the control specimen of $f_{lck} = 30$ MPa, $V_f = 1\%$ and 4D fibre with an orientation angle of 0°. Hence, it can be deduced that by increasing the orientation angle, the load increases and takes place at a larger slip. If the angle is too high and the concrete is not dense enough, the concrete can fracture and fail in a brittle manner. These findings agree with Robins et al.'s [45] study, with the exception that the fibres used in that work ruptured at a higher inclination angle. However, in the present work, the concrete fractured. This could be attributed to the enhanced tensile strength of the 4D fibres as compared to the fibres mixed in the experiments carried out by Robins et al. [45] coupled with the porous nature of LWAC, which could induce cracking and fracturing much more readily.

It is important to note that for some specimens, such as the one shown in Figure 10 with an orientation angle of 0°, the load increased to an unexpected value (in this example 590 N) before any activation of fibre pull-out. This value is thought to be overly high for concrete with a tension of $f_{lck} = 30$ MPa, which usually has a pull-out strength of $P_{max} = 244$ N. Upon the inspection of the pulled-out specimen after the test, it was observed that a lightweight aggregate positioned at the notch was split, which led to a drastic increase in the load. It was also interesting to measure that the aggregate had a diameter of almost 5 mm (Figure 11), i.e., 7 mm smaller than that of the notch, which should not force the crack to go through it. However, this can be justified, since for other material tests such as compression tests—detailed in earlier studies [30,31]—some of the aggregates were sheared through in a similar manner. In the same test, this was followed by a sudden drop in the load before fibre activation took place.

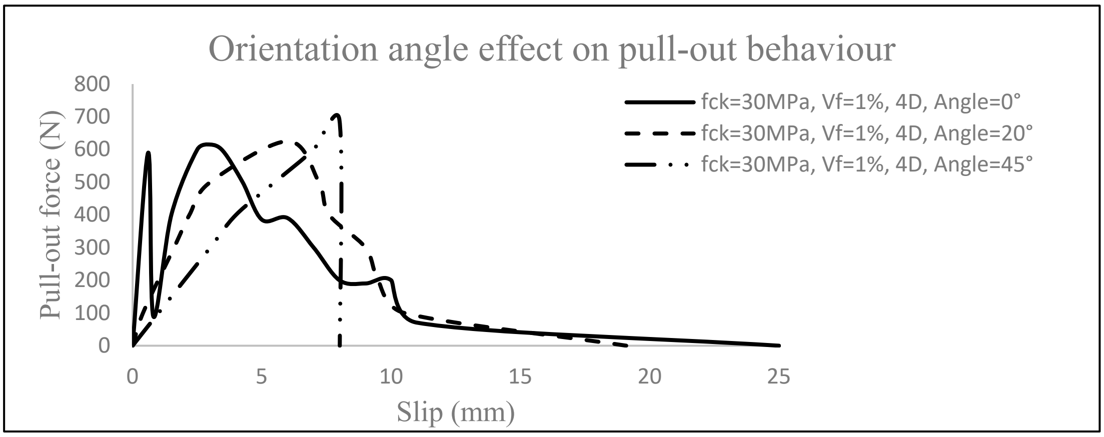

Figure 10. Pull-out load–slip behaviour with different orientation angles for 4D specimens.

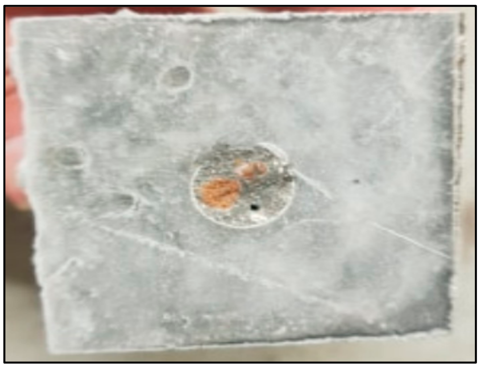

Figure 11. A pull-out specimen with a split 5 mm aggregate at the notch.

3.1.8. Adequacy of Smooth Fibres

In order to investigate the possibility of mixing lightweight concrete with straight smooth round fibres, 3D and 5D fibres with hooks being cut off were tested, and the results are depicted in Figure 12. The difference in the embedded length is due to the longer 5D hooks (about 10 mm for each hook, which resulted in 40 mm of fibre remaining in a straight length) compared to the 3D hooks (about 5 mm for each hook, which resulted in a 50 mm fibre length). For both fibres, the load dropped right after cracking at about 35–50 N, and a decay curve ensued with hardly any upgrade in load. These values agree with Alwan et al.'s [46] pull-out loads from tests with shorter straight and smooth DRAMIX fibres embedded in concretes with low strengths. Also, Abdallah and Rees [57] tested straight DRAMIX fibres embedded in concrete with a compressive strength of 33 MPa and recorded similar values. The tests in the present study demonstrate the importance of hooks in the structural responses of fibrous lightweight concrete since the hook-less 5D and 3D fibres only maintained the load until the eventual pull-out. Thus, it can be concluded that the usage of straight fibres is not recommended for lightweight concrete due to its low densification, resulting in a weak fibre–matrix interfacial bond strength, which causes smooth straight fibres to be pulled out easily.

It is important to note that for all of the preceding specimens examined according to the pull-out test, any observed upgrade in the uniaxial tensile or pull-out strength (due to the addition of fibres) might not occur in a different structural element where fewer fibres than those designed for this study are *actually* present in the vicinity of the crack. Other reasons include an insufficient embedded length and unfavourable fibre orientation angle (for example, an angle vertical to the tensile load or an angle which causes concrete fracture above 45–50°). All of these reasons can lead to lowering of the uniaxial tensile strength developed due to fibre reinforcement. By contrast, a favourable inclination angle (about 20°) and an optimum embedment length ($L_E = L_f/2$) would enhance the pull-out behaviour and energy dissipation. For this reason, fibre orientation factor η will be discussed later on to examine its effect on the post-cracking uniaxial tensile stress.

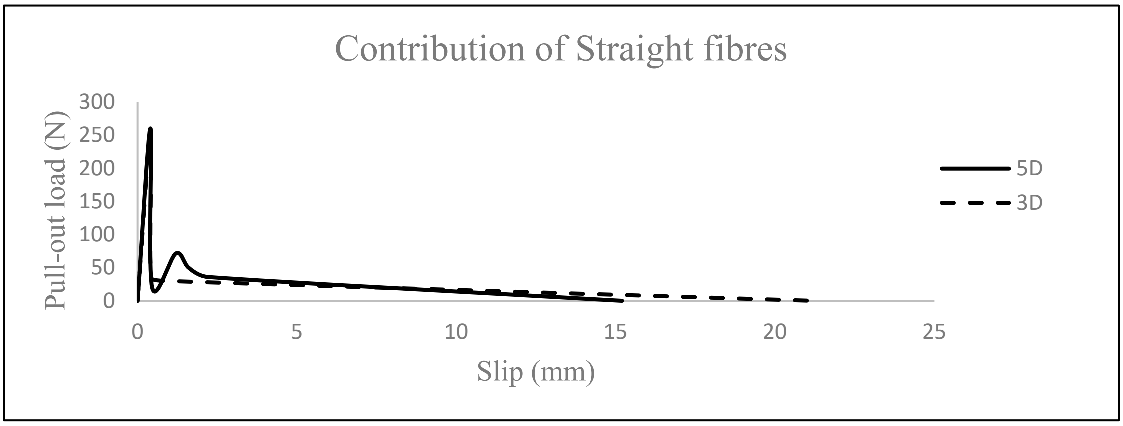

Figure 12. Pull-out load–slip behaviour of straight fibres.

3.2. Key Characteristics of the Uniaxial Tensile Behaviour of SFRLC

Table 5 summarises the key parameters defining the uniaxial tensile behaviour of fibrous composite. Each of these parameters will be discussed next.

Table 5. Assessment of pull-out behaviour. [1] Maximum tensile stress unfactored (orientation factor (η_0) = 1) of plain or fibrous concrete; [2] work performed; [3] average bond stress; [4] equivalent bond stress; [5] ultimate bond stress; [6] fibre efficiency. Standard deviations for f_{lcm} and $f_{lctm,m}$ are shown between brackets.

f_{lcm} (MPa)	V_f %	Fibre Type	$f_{lctm,m}$ [1] (MPa)	W_{total} [2] (N.mm)	τ_{av} [3] (MPa)	τ_{eq} [4] (MPa)	τ_{ult} [5] (MPa)	ξ [6]
30.1 (3.8)	0		2.16 (0.13)					
36.5 (4.2)	0		2.36 (0.17)					
44.1 (5.7)	0		2.83 (0.37)					
33.3 (4.1)	1	3D	4.17 (0.39)	1801.6	5.1	3.8	9.83	0.36
32.8 (3.3)	1	3D	4.18 (0.41)	2167.8	4.01	2.8	9.85	0.36
35.0 (4.4)	2	3D	8.96 (0.72)	4655.1				
34.9 (4.1)	1	4D	9.67 (1.02)	4085.8	8.9	4.9	16.6	0.65
34.6 (3.2)	2	4D	16.03 (1.38)	6073				
34.3 (4.7)	1	4D	9.82 (1.11)	4547.5				0.65
34.1 (4.1)	1	4D	10.85 (0.82)	2898.5				0.72
36.2 (6.2)	1	3D	5.12 (0.35)	1551.2	6.93	6.6	12.1	0.44
34.6 (4.9)	1	5D	10.41 (1.33)	6170.5	9.37	7	16.1	0.45
44.1 (5.9)	1	5D	8.17 (0.37)	2216				0.36
44.1 (6.7)	1	5D	11.08 (1.21)	3257.8	17.3	11.04	17.1	0.48
31.5 (2.1)	0.7	3D*	5.01 (0.59)	1812.8	6.2	3.3	15.2	0.58

Table 5. *Cont.*

f_{lcm} (MPa)	V_f %	Fibre Type	$f_{lctm,m}$ [1] (MPa)	W_{total} [2] (N.mm)	τ_{av} [3] (MPa)	τ_{eq} [4] (MPa)	τ_{ult} [5] (MPa)	ξ [6]
31.0 (8.1)	0.4	3D**	1.55 (0.13)	667.8	3.8	3.9	6.8	0.29
38.2 (4.9)	1.2	3D**	3.97 (0.41)	903.7				
32.4 (2.1)	1	5D	0.49 (0.08)	325	1.7	1.05	1.26	0.08
32.4 (6.2)	1	3D	0.53 (0.04)	318	0.6	0.5	0.48	0.04

3.2.1. Maximum Uniaxial Tensile Stress $f_{lctm,m}$

The maximum uniaxial tensile stress $f_{lctm,m}$ is the larger value of the uniaxial tensile stress due to plain concrete $f_{lctm,p}$ or post-cracking residual tensile stress due to fibre concrete $f_{lctm,f1}$. $f_{lctm,p}$ can be calculated using the pull-out response by dividing the P_{max} value for plain specimens by the area of the notch. To calculate the contribution of steel fibres to the tensile strength of concrete at any instant, the rule of composites is used. Thus, the actual composite stress is

$$f_{lctm,fi} = \sigma_{av,f} + \sigma_c \tag{1}$$

$\sigma_{av,f}$ and σ_c are the average stresses of the fibre and concrete, respectively.

From [26,58–60], the fibre contribution can be calculated using the following expression:

$$\sigma_{av,f} = \sigma_f V_f \eta_0 \tag{2}$$

where V_f is the fibre volume fraction, and η_0 is the fibre orientation factor taken as 0.41.

Hence, Equation (1) becomes

$$f_{lctm,fi} = \sigma_f V_f \eta_0 + \sigma_c (1 - V_f) \tag{3}$$

The classical contribution of both concrete and steel fibres in an SFRC composite remains true for SFRLC with $\sigma_f \approx 0$ before cracking and σ_c = 0 after cracking since it was demonstrated from the experiments that practically only steel fibre reinforcement contributes to tension stiffening for lightweight concrete immediately after matrix cracking. Following cracking, once the maximum pull-out strength P_{max} for a single fibre is known, the fibre stress σ_f can be readily derived using P_{max}/A_f with A_f as the area of a single fibre. Hence, at post-peak, the maximum residual stress (or first residual stress $f_{lctm,f1}$) of SFRLC can be calculated using the following equation:

$$f_{lctm,f1} = \sigma_f(\text{peak}) V_f \eta_0 = P_{max}/A_c V_f \eta_0 \tag{4}$$

$f_{lctm,m}$ is increased by the addition of fibres, an increase in V_f and an increase in the number of bends. It should be noted that the post-cracking residual tensile stress $f_{lctm,f1}$ used to derive $f_{lctm,m}$ for fibrous specimens in Table 5 is unfactored. To account for the random distribution of fibres in a 3D real fibrous concrete structural element, an orientation factor of η_0 = 0.41 is introduced [26]. The orientation factor can be defined differently in the literature (η_0 = 0.5 [61] and variable according to size effect [34]).

Figure 13 shows the uniaxial tensile strength $f_{lctm,f1}$ of the SFRLC specimens tested, normalised to the corresponding plain concrete strength of the same grade $f_{lctm,p}$. From Figure 13, the maximum SFRLC post-cracking residual uniaxial tensile strengths $f_{lctm,f1}$ reinforced with V_f = 1% were 54%, 126%, 135%, 92%, 46%, 7% and 15% of the plain concrete strength of the same grade $f_{lctm,p}$ when 3D, 4D, 5D, 3D**, 3D*, hook-less 3D and hook-less 5D fibres were added, respectively. This discrepancy in enhancing the residual fibrous tensile resistance of SFRLC between these mixes was essentially due to the effectiveness of the bond between concrete and steel fibres. In Figure 13, it can be seen that with the addition of V_f = 1%, all fibres showed a residual tension softening behaviour with the exception of 4D and 5D fibres, which exhibited a residual tension hardening behaviour. However, with the increase in V_f to 2%, 3D fibres were also able to induce a tension hardening effect based on the $f_{lctm,m}/f_{lctm,p}$ ratio being larger than 1.

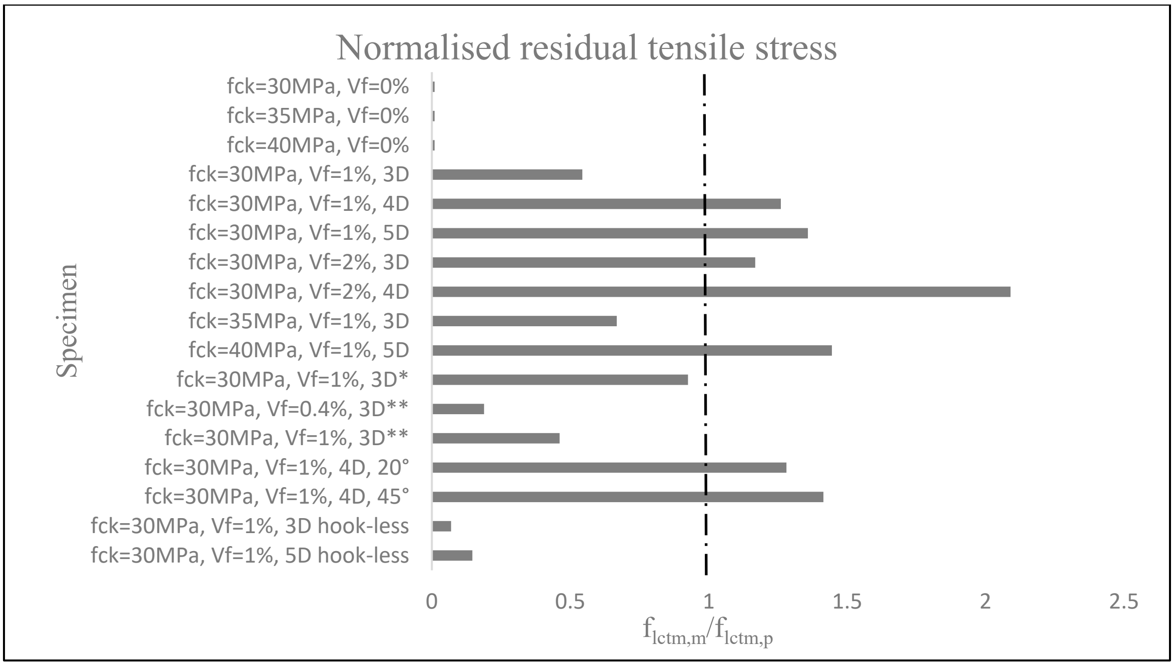

Figure 13. Normalised uniaxial tensile stress of tested specimens.

3.2.2. Pull-Out Work

Work performed is a measurement of ductility and is estimated by calculating the area under the pull-out load–slip curve. The work performed is governed by three parameters, the fibre type, fibre volume fraction and embedment length. From Table 5, it appears that the fibre type is the most influential of the three parameters. For instance, 5D fibres with V_f = 1% brought about a higher total work than 4D fibres with V_f = 2% for similar L_E and concrete strength. Hence, 5D fibres are seen to provide the highest work performed followed by 4D, 3D, 3D* then 3D**. Also, the higher the volume fraction V_f, the higher the total work performed. Moreover, clearly the larger L_E, the more the energy dissipation through fibre frictional pull-out, which in turn translates to a more ductile response of the pull-out load–slip curve.

3.2.3. Bond Strength

Several equations were developed in the past to quantify and assess the bond behaviour between fibres and concrete. The most important ones are summarised in Table 5. The average bond stress τ_{av} [53] is defined as the maximum pull-out strength divided by the initial bond area between the concrete and embedded fibre:

$$\tau_{av} = P_{max}/\pi d_f L_E \quad (5)$$

where τ_{av} (MPa) is the average fibre–matrix interfacial bond shear stress, d_f (mm) is the fibre diameter and L_E (mm) is the initial embedment length defined as the shorter length of the embedded fibre after the crack takes place at the notch in the pull-out specimen. Since the experiments conducted showed that the embedment length plays no practical role in altering the maximum pull-out strength but merely affects the frictional pull-out, the average bond strength gives a poor estimate of the bond if the latter is to be directly linked to the peak strength. The equivalent bond strength τ_{eq} [62] is defined as the fibre–matrix interfacial bond stress during the entire fibre pull-out process using the total work due to fibre pull-out:

$$\tau_{eq} = 2W_p/\pi d_f L_E^2 \quad (6)$$

where W_p (N.mm) is the total work performed by the fibre, which is equivalent to the area under the stress–slip once concrete cracking develops. The equivalent bond strength governs the effectiveness of concrete crack control and can therefore be regarded as a direct measure to evaluate the structural performance, including the ductility and ultimate loading capacity of fibrous concrete. Since P_{max} is affected only by the fibre hook contribution, then the embedded length must be at least $L_E = L_e = L_h + 5d_f$ for complete fibre hook straightening. It should be noted that a higher value of the embedded length $L_E > L_e = L_h + 5d_f$ will not increase the pull-out strength, as shown previously. Equation (4) is rearranged to become

$$P_{max} = \tau_{ult}\pi d_f(L_h + 5d_f) \quad (7)$$

Hence, the ultimate bond strength of the SFRLC composite with hooked-end fibres can be written as

$$\tau_{ult} = P_{max}/\pi d_f(L_h + 5d_f) \quad (8)$$

The ultimate bond strengths for the fibres mixed with different lightweight concrete grades are summarised in Table 5. It should be noted that for the hook-less 3D and 5D fibres, L_h was taken as the total embedded length.

It can be seen from the experimental data that 4D fibres resulted in the highest ultimate bond strength, therefore exceeding both 3D and 5D ultimate bond strengths for the same concrete grade of f_{lck} = 30 MPa. On the other hand, 3D** developed the lowest bond strength amongst hooked-end fibres. Also, it should be noted that by increasing the concrete grade, the ultimate bond strength increased as well. This was seen for the 5D and 3D specimens tested with f_{lck} = 30 and 40 MPa. In addition, 3D* fibres with an L_f/d_f = 80 aspect ratio developed an average bond strength 55% higher than that of 3D fibres with L_f/d_f = 65. Hence, for DRAMIX hooked-end fibres, the high aspect ratio brings about a higher bond strength. Lastly, the lowest bond strength was calculated for the smooth straight fibres (i.e., hook-less fibres).

3.3. Fibre Optimisation

In order to determine the fibres that are best suited for reinforcing the lightweight concrete tested, a brief optimisation study was carried out and is discussed next.

3.3.1. Fibre Stress Efficiency

The fibre stress efficiency values are summarised in Table 5. Fibre efficiency is a direct measure of the effectiveness of fibre reinforcement for a particular concrete. A very low value indicates an under-performance of fibre reinforcement, while a very high value may indicate over-performance of fibre reinforcement, which may lead to fibre rupture. Also, fibre efficiency can be a direct measure for the calculation of the formation of plastic hinges and the straightening of fibres. Fibre stress efficiency ξ is calculated by dividing the maximum stress by the ultimate stress of the fibre. Amongst all the fibres tested, the 4D and 3D* fibres showed the highest fibre stress efficiency, followed by the 5D, 3D, 3D**, hook-less 3D and 5D fibres. Since the 3D, 3D* and 3D** fibres have roughly identical hook shapes and sizes, the higher aspect ratio and fibre length are therefore the most responsible parameters for developing fibre stress efficiency given that the concrete strength is kept constant. Increasing the inclination angle led to a greater fibre efficiency, as seen with the

4D fibres; however, this could cause concrete fracture for the porous lightweight concrete matrix. A higher concrete grade, which means a lower w/c ratio and a denser concrete matrix, would bring about a better bond, which in turn would result in a higher fibre stress efficiency. Lastly, L_E played no factor in increasing the fibre stress efficiency.

3.3.2. Fibre Energy and Bond Indices

In order to further investigate the behaviour of SFRLC for fibre optimisation, an assessment of energy dissipation and bond strength is vital. Qi et al. [55] aimed to choose the fibre type that is the most suitable for the concrete tested by defining both the energy dissipation index η_f and bond strength index ζ_f using a single fibre pull-out test.

$$\eta_f = W_p / A_f L_f \tag{9}$$

$$\zeta_f = \tau_{av} / A_f L_f \tag{10}$$

However, these two equations need adjustment of the accuracy of their mechanical meaning based on the pull-out tests carried out previously. This is the case because it was shown that the fibre length L_f plays no role in enhancing the bond strength and plays a minimal role in energy dissipation when compared to L_E. Therefore, Equations (9) and (10) become

$$\eta_{f,actual} = W_p / A_f L_E \tag{11}$$

$$\zeta_{f,actual} = \tau_{ult} / A_f (L_h + 5d_f) \tag{12}$$

Figure 14 shows the normalised actual efficiency indices, which are calculated by dividing the actual efficiency indices by the control 3D specimen actual efficiency indices. It can be seen that the more extensive the hooks, the higher the energy dissipation efficiency index. Consequently, the 5D and 4D fibres showed the highest energy efficiency indices due to longer hooks, which increase energy dissipation. Also, the higher the aspect ratio for a similar fibre length, the higher the energy dissipation efficiency index, as can be seen with the 3D* fibre (a_f = 80) compared to the 3D and 3D** fibres, which have a similar aspect ratio (a_f = 65). The fibre bond strength efficiency index varies, with the 3D* fibre having the highest value and the 3D and 5D fibres showing the lowest values.

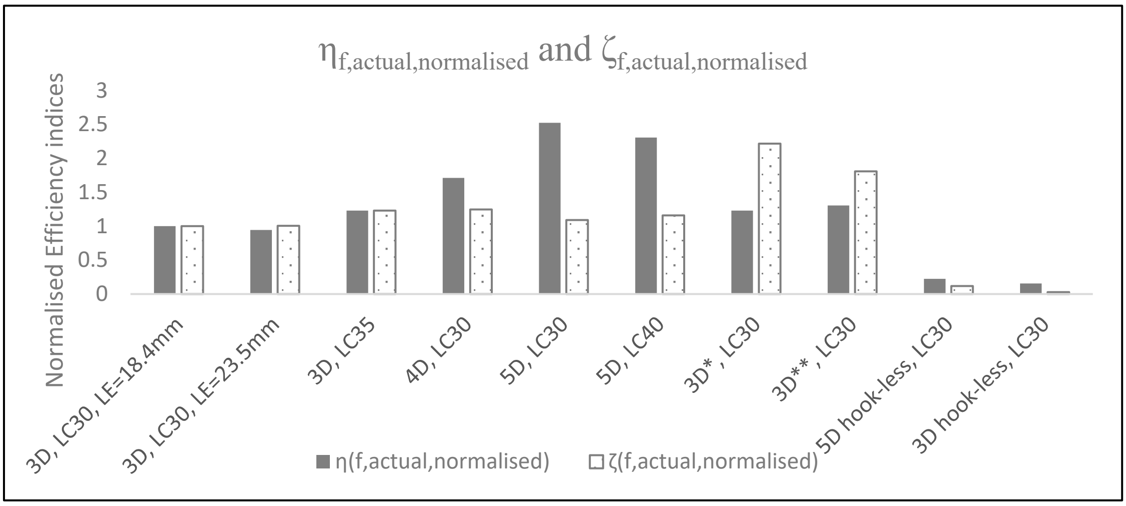

Figure 14. Normalised actual efficiency indices for pull-out specimens tested.

3.3.3. Fibre Plasticity Study

As shown in Figure 8, all fibres appeared to be straightened and then pulled out of the lightweight concrete notched prisms with the exception of some 5D specimens. When the 5D fibres were not fully straightened, a local fracturing of the matrix followed, which is an unfavourable mode of failure. When fibres are not fully straightened, a lack of full plastic hinges are developed, which is why the 5D fibre stress efficiency was low. To this end, the fibre tensile stress was thought to play a secondary role in the behaviour of the pull-out specimens; however, the high yield stress of the 5D fibres combined with the hook geometry and angles (summarised in Table 1) are thought to play a negative role in preventing steel yielding of fibre and thus increase the possibility of fracture. To investigate the latter, Alwan et al.'s [46] pulley model, depicted in Figure 15, was adopted to determine the magnitude of the load causing the plastic hinges to form before hook straightening. This theoretical pull-out load was then compared to the corresponding experimental one.

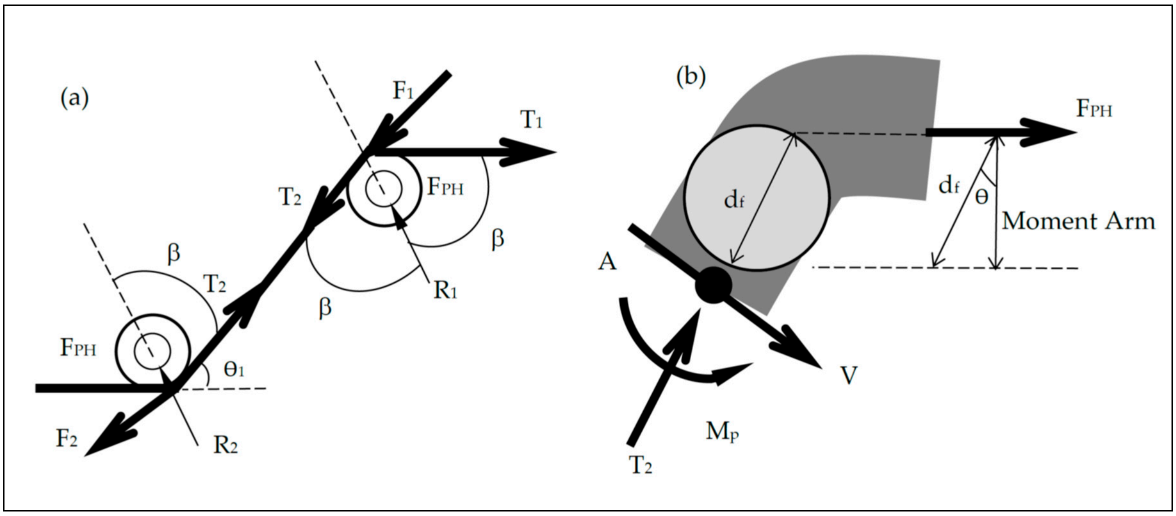

Figure 15. (**a**) Pulley model for 3D fibres and (**b**) FBD for plastic hinge at fibre hook (adapted from [46,47]).

In Figure 15, F_{PH} corresponds to the cold work needed to straighten the steel fibre at the location of the plastic hinge, M_p is the plastic moment of the steel fibre and T_2 is the chord tension in the fibre. Since the purpose of this section is to determine the force required to develop a plastic hinge and straighten the fibre, F_{PH} was calculated for 3D, 4D and 5D fibres.

For point A,

$$F_{PH} = M_p / d_f \cos\theta \quad (13)$$

The plastic moment M_p is suggested by Alwan et al. [46], who carried out pull-out experiments on 3D DRAMIX fibres embedded in concrete with w/c ratios ranging from 0.5 to 1.0. In Alwan et al.'s study [46], the pull-out loads were around 150–180 N for 3D fibres with an aspect ratio of 0.6 (d_f = 0.5 mm, L_f = 30 mm), which are comparatively higher than the pull-out loads recorded in this work for the 3D** fibre with d_f = 0.55 mm and L_f = 35 mm, whose pull-out loads were around 90–105 N. The plastic moment in [46] is

$$M_P = f_y \cdot \pi r_f^2 / 2 \cdot d_f / 3 \quad (14)$$

where r_f is the radius of the fibre. It should be noted that Equation (14) was thought to be suitable for concrete where an elastic–plastic condition is sufficient for fibre pull-out. Abdallah et al. [47] suggested the following plastic moment and criticised that Equation (14) underestimates the pull-out for ultra-high-strength concrete:

$$M_P = f_y \cdot \pi r_f^2 / 2 \cdot d_f / 3 \cdot \pi / 4 \quad (15)$$

Based on Alwan et al.'s [46] theoretical hooked-end 3D fibre pull-out process depicted in Figure 16 (which agrees with the current experimental study), the maximum pull-out load is

$$P_{max} = P_2 = P_1 + \Delta P' = P_1 + T_1 \quad (16)$$

where $\Delta P'$ or T_1 is the contribution of plastic hinges to the pull-out load and P_1 is the pull-out load at the onset of complete debonding. P_{max} or P_2 can be found in Table 4. The total number of possible plastic hinges is 2, 3 and 4 for 3D, 4D and 5D fibres, respectively. Since hooked-end and straight fibres' pull-out behaviour shares only the pull-out load up to complete debonding P_1 [47], then according to the tests carried out on DRAMIX hooked-end fibres, P_1 = 30–55 N. P_1 could also be calculated according to the analytical study by Naaman et al. [63], but this is outside the scope of this work.

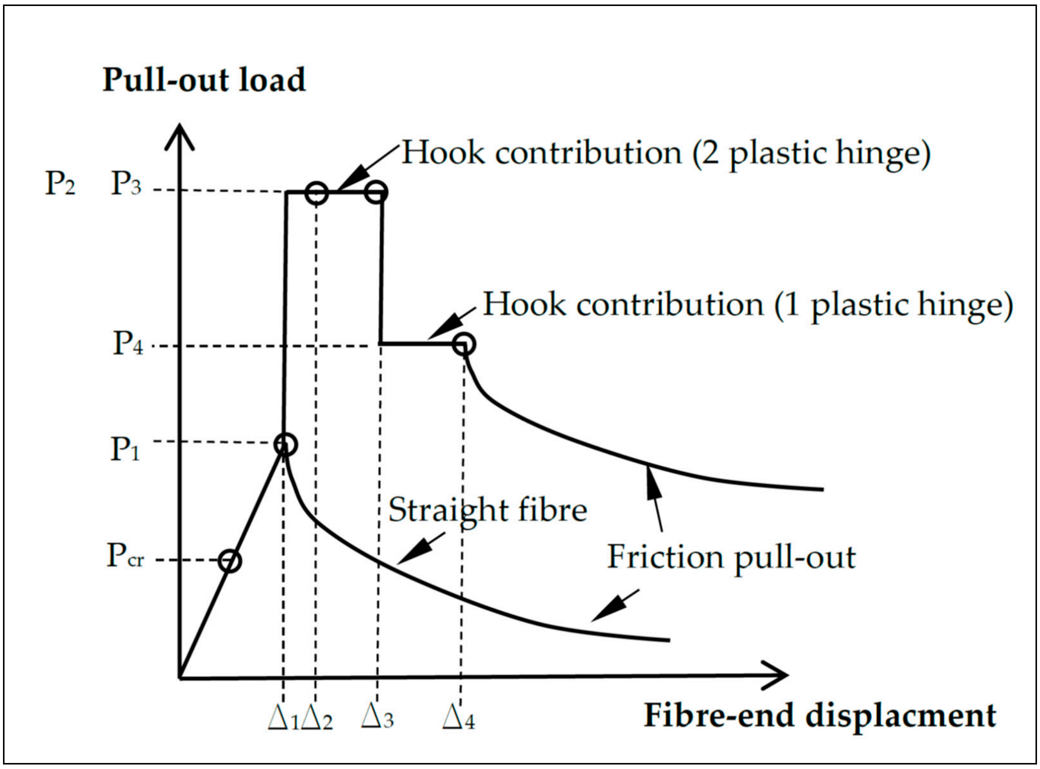

Figure 16. Sketch of theoretical hooked-end 3D fibre pull-out method adapted from [46].

The pull-out load due to plastic hinges T_1 can be calculated for 3D fibres [46] as follows:

$$T_{1(3D)} = 2F_{PH}\left[1 + \frac{\mu \times \cos\beta}{1 - \mu \times \cos\beta}\right] / 1 - \mu \times \cos\beta \quad (17)$$

μ is the coefficient of friction between concrete and steel, taken as 0.5, and β was measured, and the results are shown in Table 1. Using Equation (17), F_{PH} can be calculated and compared to that calculated using Equation (13). If the experimental F_{PH} value from Equation (17) is higher than the theoretical one calculated using Equation (13), then the fibre was straightened following the formation of two plastic hinges for 3D fibres.

Abdallah et al. [47] adapted this model to 4D and 5D fibres.

Equation (16) remains valid for both 4D and 5D fibres since the P_1 load was similar. By applying the pulley model in a similar manner to Equation (17), as depicted in

Figures 17 and 18, the pull-out load due to plastic hinges T_1 can be calculated for 4D and 5D fibres as follows:

$$T_{1(4D)} = F_{PH}\left[3 + \left(\frac{2\mu \times \cos\beta}{1-\mu \times \cos\beta}\right)\left[2\left(1+\frac{\mu \times \cos\beta}{1-\mu \times \cos\beta}\right)+1\right]\right]/1-\mu \times \cos\beta \quad (18)$$

$$T_{1(5D)} = F_{PH}\left[4 + \left(\frac{2\mu \times \cos\beta}{1-\mu \times \cos\beta}\right)\left[3+2\mu\cos\beta\left[2\left(1+\frac{\mu \times \cos\beta}{1-\mu \times \cos\beta}\right)+1\right]+2\left(1+\frac{\mu \times \cos\beta}{1-\mu \times \cos\beta}\right)+1\right]\right]/1-\mu \times \cos\beta \quad (19)$$

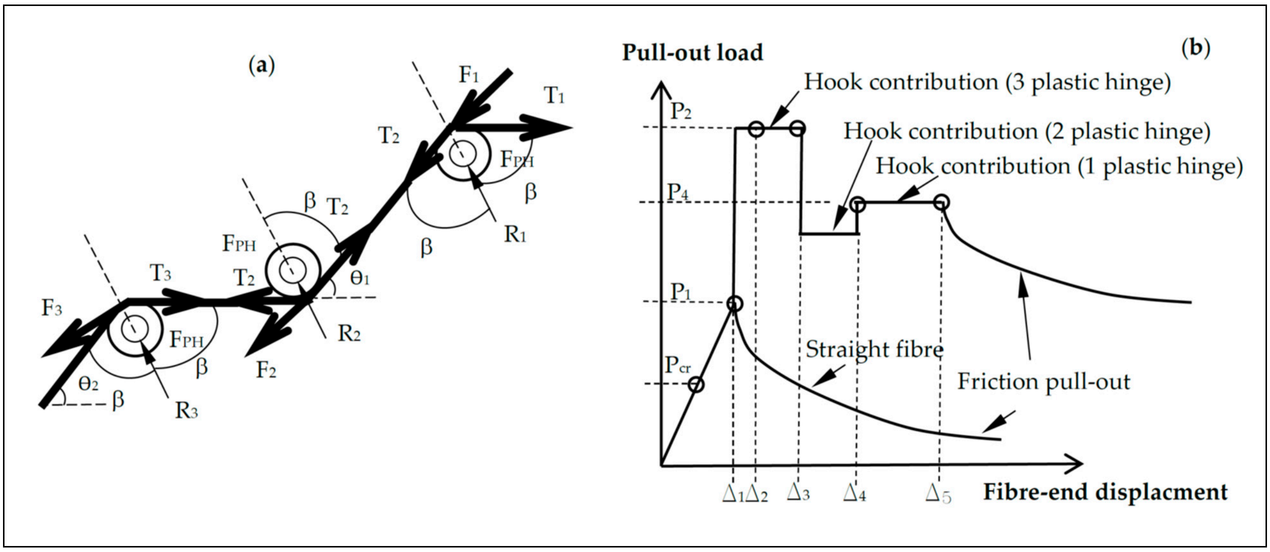

Figure 17. (**a**) Pulley model for 4D fibres; (**b**) theoretical hooked-end 4D fibre pull-out load–slip, adapted from [47].

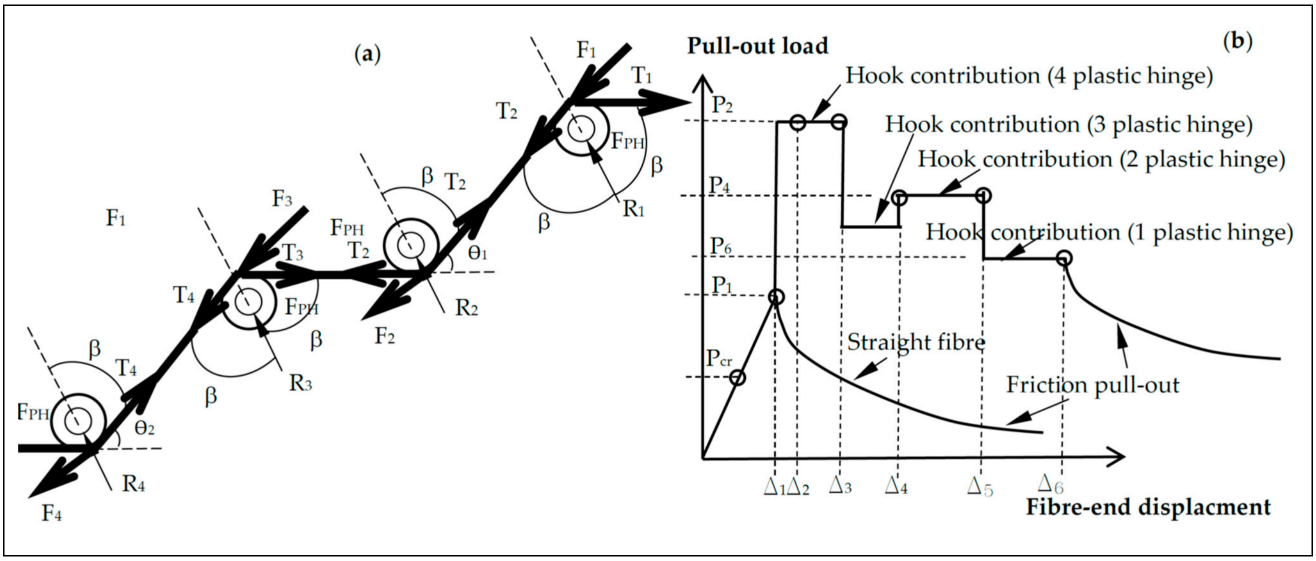

Figure 18. (**a**) Pulley model for 5D fibres. (**b**) Theoretical hooked-end 5D fibre pull-out load–slip, adapted from [47].

Table 6 shows that the theoretical model used to calculate M_p in Equation (14) suggested by Alwan et al. [46] seems to overestimate the behaviour of pull-out since $F_{PH,theoretical} > F_{PH,test}$ for all fibres, which translates into fibres not becoming straightened at the end of the test. Given that all fibres with the exception of the 5D fibre were straightened by the end of the test, a new Equation (20) was proposed to calculate M_p, which considers the comparatively weak lightweight concrete and its porous nature. This equation assumes that the effective distance between the centroids of tension and compression forces in a plastic stress distribution diagram for a steel fibre circular section is $\frac{2r_f\pi}{15}$ ($\frac{2r_f}{3}$ for Alwan et al.'s [46] model, and a true distance of $\frac{8r_f}{3\pi}$ for Abdallah et al.'s [47] model). Thus, for porous lightweight concrete, the fibres were assumed to not undergo heavy straining after developing plastic hinges before becoming straightened and eventually being pulled out.

$$M_P = f_y \cdot \pi r_f^2/2 \cdot d_f/3 \cdot \pi/5 \tag{20}$$

Table 6. Summary of experimental and theoretical F_{PH} values.

Type of Fibre	$F_{PH,test}$ (N)	$F_{PH,theoretical}$ (N) Alwan et al. (1999)	$F_{PH,theoretical}$ (N) Proposed
3D	73.8	117.6	72.1
3D**	31.5	42.8	31.1
4D	131.2	214.2	129.7
5D	90.5	265.4	166.7

As seen in Table 6, the new model marginally underestimates the value of F_{PH} by a maximum of 3% for 3D, 3D** and 4D fibres while predicting that they become straightened ($F_{PH,theoretical} < F_{PH,test}$). On the other hand, the 5D fibre clearly does not become straightened according to this model. It should be noted that while the majority of 5D specimens appeared to be completely unstraightened, some 5D specimens looked partially straightened.

Considering the preceding discussion, it is safe to assume that unless the concrete is of high strength and therefore capable of providing a strong fibre–matrix interfacial bond, such as the ultra-high-strength concrete tested by Abdallah et al. [42,47,48], it is recommended that multiple-bend fibres with a high tensile strength (such as 5D fibres) should not be employed as reinforcement for concrete with a low concrete grade since they might cause local fracturing during the fibre straightening process. Given that there exists a possibility of matrix fracture due to 5D fibres not fully developing plastic hinges and becoming straightened, 4D and 3D* fibres appear to be the most efficient fibres for use in the LWAC sample tested depending on their structural usage, with the aspect ratio a_f playing a significant role in bond strength efficiency and the number of hooks having a greater impact on the energy dissipation efficiency. Finally, it could be argued that 4D fibres with a higher a_f value would further increase the efficiency indices and thus enhance the behaviour of SFRLC.

3.4. Proposed Constitutive Tensile σ-ω Model

Although it cannot be used directly for engineering calculations such as beam section analysis, the tensile stress–crack width (σ-ω) relationship is preferred to the stress–strain (σ-ε) relationship because it represents the actual behaviour of the fibrous material, especially after cracking. It is derived from analysing the output results of the uniaxial tensile test, is independent of the member size effect, and can be directly applied from the pull-out tests used for FEM [64]. Also, the σ-ω relationship can provide the information needed to design the serviceability limit state, including fatigue and shrinkage. To be able to use the σ-ε relationship for section analysis based on pull-out tests, the strain values are derived using the crack width and the structural characteristic length l_{cs} (using the relation $\varepsilon = \omega/l_{cs}$), which varies depending on the specimen size, V_f, fibre type, reinforcement, loading level and matrix strength. No agreement has been achieved to determine l_{cs}; however, for beams, l_{cs} can be chosen as the minimum of s_{rm} and h_{sp}, where s_{rm} is the mean distance between cracks and h_{sp} is the unnotched depth [64,65]. It should be noted that the proposed model ignores the slight drop in load following matrix cracking, which lasted in the range of

0.05 to 0.1 mm slip before the load was increased. This was deemed to have a negligible practical impact on the accuracy of the σ-ω relationship. Figure 19 depicts the idealised proposed multilinear stress–crack width relationship based on the uniaxial tensile pull-out tests for 3D fibres.

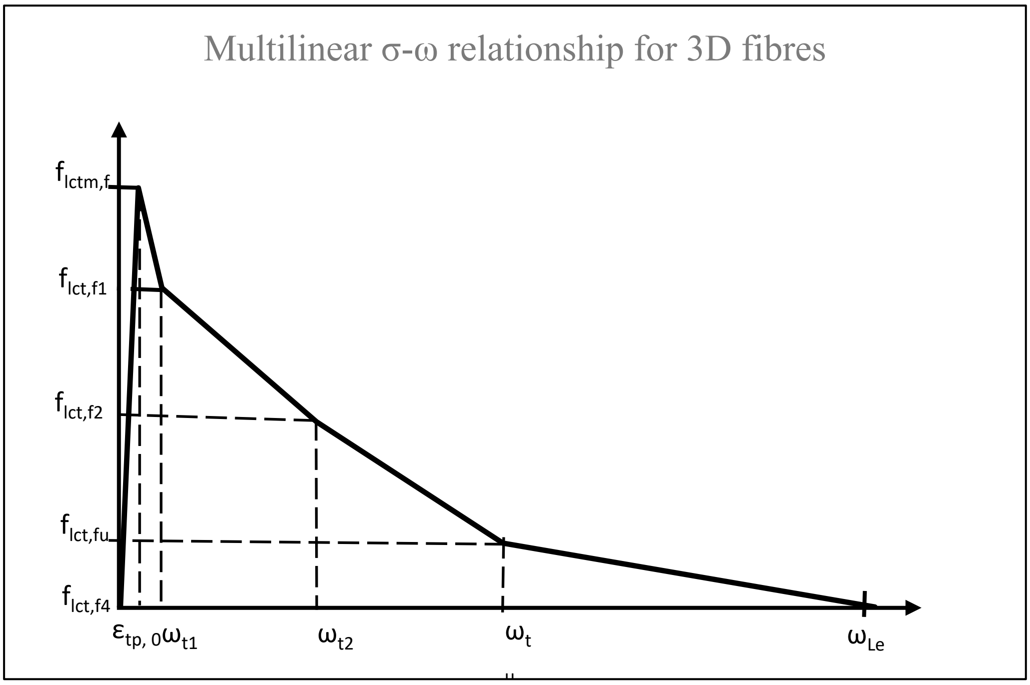

Figure 19. Multilinear σ-ω relationship for 3D fibres.

Due to the sensitivity of the pull-out machine, the accuracy of measuring the early slip pre-peak was somewhat limited. Hence, the rule of fibrous composites was adopted to determine the strain at peak before cracking for plain concrete ε_{tp}. The Young's modulus of elasticity of the concrete in tension is as follows:

$$E_{ct} = E_{mt}V_m + \eta_l\eta_o E_f V_f \quad (21)$$

where E_{mt} and E_f are the plain concrete matrix and the fibre's Young's moduli of elasticity in tension, respectively; V_m and V_f are the volume fractions of the matrix and fibres, respectively; η_l is the fibre length efficiency; and η_0 is the fibre orientation factor.

Similarly to Lok and Xiao [59], it is assumed that the initial modulus of elasticity in tension is equal to that in compression. Hence,

$$E_{mt} = E_c \quad (22)$$

Also, based on the pull-out tests, it was evident that σ_f was low since a relatively negligible increase or decrease in the uniaxial tensile strength of the concrete was recorded pre-crack for fibrous concrete specimens. Once cracking took place, the load abruptly degraded, followed by mobilisation of the fibre crack arresting effect. Therefore, before cracking takes place, Equation (21) with $V_m \sim 1$ becomes

$$E_{ct} \approx E_c \quad (23)$$

The strain at peak can now be calculated as shown below, where $f_{lctm,p}$ is the stress of the plain concrete.

$$\varepsilon_{tp} = f_{lctm,p}/E_{ct} \quad (24)$$

As previously shown in the pull-out tests, the uniaxial tensile stress at which the crack took place for SFRLC was similar to that of the plain lightweight concrete. The stress due to fibres immediately before cracking can be estimated using the following equation:

$$f_{lctm,f0} = f_{lctm,p} \tag{25}$$

Plain lightweight concrete uniaxial tensile stress can be written as

$$f_{lctm,p} = 0.26 f_{lcm}^{2/3} \times (0.4 + 0.6\rho/2200) \tag{26}$$

Equation (26) was adapted from Eurocode 2 [66], where f_{lcm} (MPa) is the mean compressive strength of lightweight concrete based on the cylinder compression tests, and ρ is the oven density of concrete (kg/m^3). Using the above equation, R^2 was found to be 0.96.

From Figure 19, the first residual uniaxial tensile stress $f_{lct,f1}$ of SFRLC, which takes place after cracking as peak of either tension hardening or softening, can be derived using Equation (4) from the pull-out test or regression Equation (27) (R^2 = 0.95). The crack width ω_{t1} at $f_{lct,f1}$ varied for all the SFRLC specimens, with specimens having stronger fibres showing the highest ω_{t1} values. For the majority of specimens, the ω_{t1} value ranged from 0.4 to 0.5 mm for 3D fibres, 0.5 to 0.8 mm for 4D fibres and 1.1 to 1.4 mm for 5D fibres. This largely agrees with Abdallah et al.'s [57] results of pull-out tests on normal strength concrete of 33 MPa. The residual slip ω_{t1} can also be calculated based on the following regression Equation (28) (R^2 = 0.89). The fibre reinforcing factor $\rho_f = V_f(L_f + L_e)/d_f(\delta \cdot \kappa)$ is detailed elsewhere, and $\rho'_f = \rho_f$ (for V_f = 1%).

$$f_{lct,f1} = \eta_0 V_f f_{lctm,p} \rho'_f \left(172.1 + 35.5 f_{lctm,p} \rho'_f\right) \tag{27}$$

$$\omega_{t1} = 0.2124 {\rho'_f}^2 + 0.3775 \rho'_f \tag{28}$$

Using the idealised stress–crack width relationship in Figure 19, the load drops at a further slip of 2 mm to 3 mm. This was denoted as $\omega_{t2.}$ After thorough inspection of the pull-out tests, ω_{t2} was deemed to be approximately equal to the hook arm L_2 shown in Figure 2. The observation that $\omega_{t2} = L_2$ is also supported by the work carried out on hooked end fibres in [46] and recent revisions from Abdallah et al.'s [57] pulley model on DRAMIX hooked-end 3D, 4D and 5D fibres. In the latter study, after fibre debonding, two plastic hinges were developed for 3D fibres (three plastic hinges for 4D fibres and four plastic hinges for 5D fibres). At this stage, the second residual pull-out stress due to fibre contribution was recorded. Once the slip reaches L_2, the mechanical anchorage mechanism becomes supported by only one plastic hinge for 3D fibres, two hinges for 4D fibres and three hinges for 5D fibres, which results in a significant drop in the pull-out load. From the pull-out tests, the second residual pull-out stress $f_{lct,f2}$ recorded at $\omega_{t2} = L_2$ was 30 to 40% lower than $f_{lct,f1}$ for the 3D, 4D and 5D specimens. Thus, for design purposes,

$$f_{lct,f2} = 0.60 \times f_{lct,f1} \tag{29}$$

When the crack width $\omega_{tu} = L_h$ (the full length of the hook), the load drops significantly, and only frictional pull-out becomes responsible for the SFRLC behaviour, while one plastic hinge and two plastic hinges remain responsible for the behaviours of 4D and 5D fibres, respectively. Hence, at $\omega_{tu} = L_h$, the load drops to about 10 to 25% for all the specimens tested and frictional pull-out starts to take place. Thus, the stress $f_{lct,fu}$ can be written as

$$f_{lct,fu} = 0.10 \times f_{lct,f1} \tag{30}$$

It is vital that the hook of the fibre is fully embedded in concrete for the fibrous mix to develop the maximum residual stress $f_{lct,f1}$; hence, the final crack width can be written as

$$\omega_{Le} = L_e = L_h + 5d_f \tag{31}$$

where ω_{Le} is the effective length crack width in mm. For design purposes the ultimate tensile strength $f_{lct,f4}$ can be assumed to be 0.

A similar semi-empirical approach can be adopted to derive the tensile behaviour of 4D and 5D fibres. The proposed multilinear uniaxial tensile σ-ω relationships suggested are specific to the type of fibre used and depend on experimental strength reduction factors fully based on pull-out tests. Hence, these reasons render the models laborious and reliant on uniaxial tensile tests. In order to make the model more generic (covering hooked-end, crimped or straight fibres embedded in concrete matrices with different strengths) and easy to use, and to avoid any reliability on the pull-out or uniaxial tensile tests, the generic model shown in Figure 20 is suggested.

The tensile stress in Figure 20 is explained in the equations below.

$$f_{lct} = \begin{cases} E_{ct} \cdot \varepsilon_t & \text{if } \varepsilon_t \le \varepsilon_{tp} \\ f_{lctm,f0} + (f_{lct,f1} - f_{lctm,f0})\omega_t/\omega_{t1} & \text{if } 0 < \omega_t \le \omega_{t1} \\ f_{lct,f1} e^{-\zeta} & \text{if } \omega_{t1} < \omega_t \le \omega_{tu} \end{cases} \tag{32}$$

$$\zeta = (\omega_t - \omega_{t1})/\omega_{tu} \cdot n_b/\rho_f \tag{33}$$

The tensile stress should be 0 at ω_{Le}. ω_{tu} is the L_h value for hooked-end fibres, and the length of one wave or the turn of crimped fibres and the length of a straight fibre is 10. n_b is the number of bends in one hook (one for 3D, two for 4D and three for 5D). n_b is taken as half the total number of waves for crimped fibres (usually four or three), and there are five waves for straight fibres.

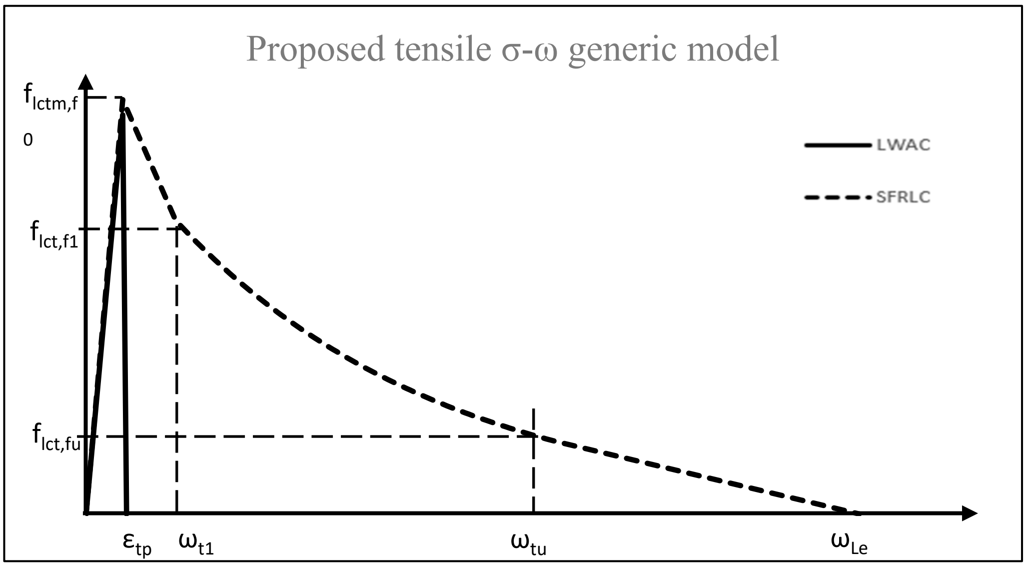

Figure 20. Proposed generic constitutive σ-ω model for plain and fibrous lightweight concrete.

3.5. Validation of Tensile σ-ω Model

In order to validate the proposed model shown above, the average experimental uniaxial tensile behaviours of 3D, 4D and 5D fibrous specimens are shown against the predictions of the proposed model presented in Figure 21.

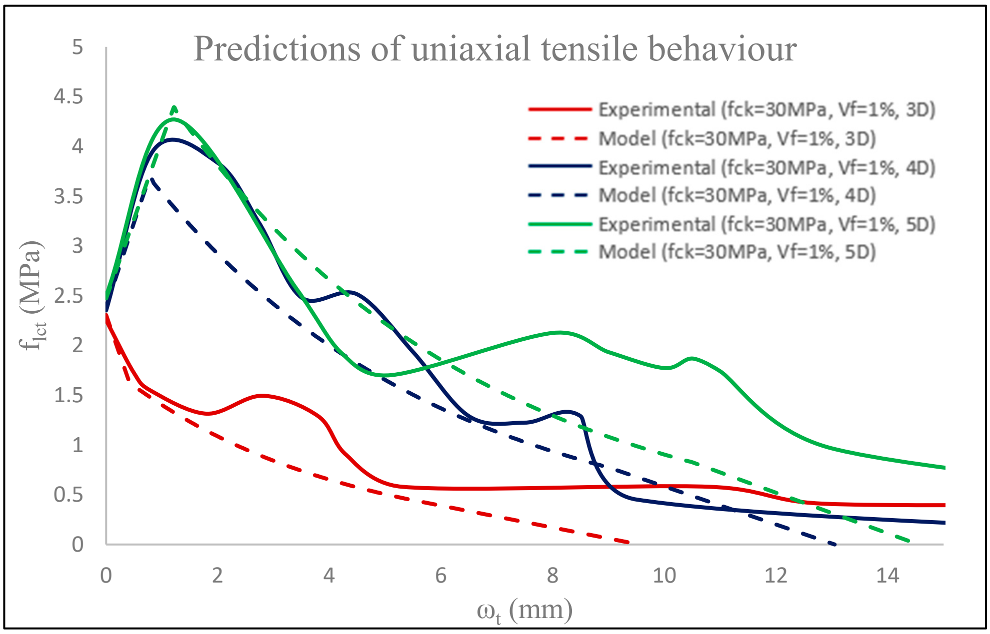

Figure 21. Predicted behaviour of uniaxial tension for 3 different specimens.

It can be seen that the proposed tensile σ-ω model predicted the uniaxial tensile behaviour of different fibrous specimens with good accuracy. For 3D and 4D specimens, the first residual tensile stress $f_{lct,f1}$ was underestimated by 4% and 6%, respectively, while for the 5D specimen, an overestimation of 2% was noted. The predicted slip ω_{t1} was within 20% of the actual one. However, this inaccuracy in slip predictions was on the conservative side and can be blamed on the high variability in slip results stemmed from the nature of the pull-out test. This observation was also reported by Barragán et al. [56], who conducted uniaxial tensile tests on SFRC (3D fibres) cylinders with comparable strengths of 30 MPa to the notched prisms tested. The proposed constitutive model assumes that the ultimate crack width is the minimum required for the adequate embedment of hooks (equivalent to the effective embedment length $\omega_{Le} = L_e = L_h + 5d_f$), which enables the development of the bond required to fully straighten the fibres. For this reason, the final slip predictions were conservative as the experimental uniaxial tensile behaviour was based on pull-out specimens with an embedment length L_E of around 25 mm, which is larger than L_e. Hence, although conservative at post-peak, the suggested model is seen to be successful in predicting the tensile σ-ω behaviour of the tested specimens.

As previously discussed in Section 2, only a handful of studies on the uniaxial tensile stress–strain or stress–crack width behaviour of SFRLC exist. De Montaignac et al.'s [64] work on the tensile behaviour of SFRC notched cylinders was investigated. De Montaignac et al. [64] carried out uniaxial tensile notched cylinders tests according to RILEM TC 162-TDF [41] on normal weight concrete with a strength ranging from 45 to 63 MPa reinforced with 3D** and 3D* fibres and generated uniaxial tensile σ-ω curves. Although, the concrete was not lightweight, it is interesting to check the reliability of the proposed uniaxial tensile σ-ω law since it mainly depends on the type of fibre and the plain concrete strength, which were outlined by De Montaignac et al. [64].

Figure 22 shows the proposed constitutive model prediction of the experimental notched cylinders' uniaxial tensile σ-ω behaviour for concrete reinforced with 3D* fibres and V_f = 1% from the study by De Montaignac et al. (2011). It is evident that the proposed model was successful in predicting the uniaxial tensile behaviour of SFRC. The model underestimated the peak post-cracking tensile stress by only 3% and overestimated the residual stresses by an average of 5–10% with a crack width of 1.9 mm.

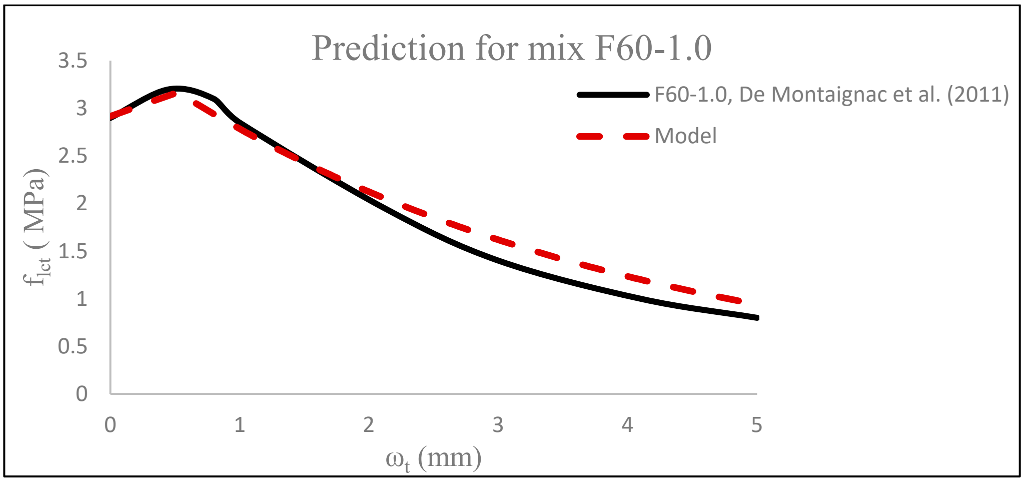

Figure 22. Prediction of [64] uniaxial stress–crack width behaviour of SFRC notched cylinders reinforced with 3D* fibres with V_f = 1%.

Figure 23 shows the proposed constitutive model prediction of the experimental notched cylinders' uniaxial tensile σ-ω behaviour for concrete reinforced with 3D** fibres and V_f = 1% from the study by De Montaignac et al. [64]. As previously noted, the proposed model ignored the dip in stress, which takes place at a 0.1 mm slip after cracking, commonly observed in uniaxial tests such as this one and that in [56]. This should have little to no effect on the prediction of the behaviour of the load deflection of structural elements using the structural characteristic length l_{cs} to derive the strain (such as in [65]). The proposed constitutive σ-ω model predicted the uniaxial tensile behaviour of SFRC with good accuracy and was conservative by an average of 8–12% at all levels.

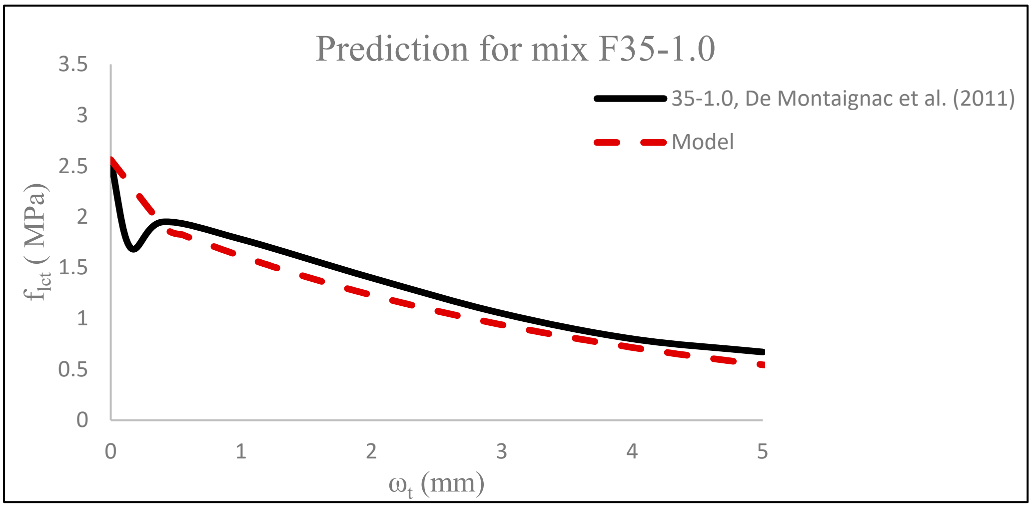

Figure 23. Prediction of [64] uniaxial stress–crack width behaviour of SFRC notched cylinders reinforced with 3D** fibres of V_f = 1%.

3.6. Fracture Energy G_f

Using the proposed tensile constitutive σ-ω relationship based on the pull-out experiments, the fracture energy of the fibrous mixes can be calculated as follows:

$$G_F = \int_{\omega_c = 0}^{\omega_{L_E}} f_{lct}(\omega) dw \quad (34)$$

The G_F values for each of the mixes are summarised in Table 7 for concrete with f_{lck} = 30 MPa. It could be observed that the main reasons behind the differences in G_F

values are the number of bends n_b, fibre hook length and fibre volume fraction. The larger the n_b, hook length and V_f, the more energy is absorbed to deform and straighten the fibre, and hence, the higher the fracture energy G_F produced per unit width of crack. From Table 7, it can be seen that the highest G_F value is generated by samples with 4D and 5D fibres, while those with 3D** fibres generated the lowest G_F values. It was not possible to calculate the fracture energy for plain lightweight concrete as the machine was not stiff enough to record the insignificant crack width recorded following concrete cracking using the uniaxial tensile pull-out test.

Table 7. Fracture energy based on proposed constitutive uniaxial tensile model.

Fibre Type	V_f	G_F (N/mm)
3D	1%	5393
	2%	13,253
4D	1%	17,433
	2%	44,892
5D	1%	23,563
	2%	60,589
3D*	1%	9389
	2%	22,045
3D**	1%	4872
	2%	11,654

3.7. Conclusions

In the present experimental investigation, a direct tensile test was designed to examine the pull-out load–slip and uniaxial tensile behaviour of recycled lightweight aggregate concrete. Several parameters were included in the study, such as fibre geometry (n_b, a_f, and L_f), volume fraction V_f and compressive strengths f_{lck}. It can be concluded that

- The designed pull-out test showed a truer representation of a tensile crack being bridged by fibres on the macro level in a structural member. Also, using the area of the notch in which the fibre(s) was embedded, it was possible to regard the pull-out test as a uniaxial tensile test of plain and fibrous lightweight concrete.
- Due to the absence of a natural tension-stiffening mechanism, plain lightweight concrete was found to fail in a sudden brittle manner once it reached its peak tensile strength. The addition of fibres to lightweight concrete was seen to drastically enhance both the tensile strength and ductility, including work and fracture energy, once the main tensile crack was initiated. Before the latter took place, a negligible increase in strength was seen. The higher the number of fibre bends n_b and the higher the fibre aspect ratio a_f, fibre length L_f, fibre dosage V_f and plain concrete compressive strength f_{lck}, the higher the post-cracking tensile strength and ductility of the fibrous composite. The embedded length L_E was found to only enhance the ductility of SFRLC. It was found that a minimum value of $L_E = L_h + 5d_f$ is required for hooked-end fibres to bond adequately and achieve a maximum pull-out load P_{max}. Also, although the increase in the fibre inclination angle θ_f was found to increase the post-cracking tensile strength as compared to $\theta_f = 0°$, in some instances where $\theta_f = 45°$, the concrete fractured. An inclination angle of about 20° was found to add tensile strength without compromising ductility. It was found that smooth fibres were ineffective at increasing the strength of SFRLC and merely enhanced ductility via frictional pull-out.

- A new ultimate bond strength equation to quantify the behaviour of hooked-end steel fibres in lightweight concrete was suggested based on the pull-out tests. It was found that 4D fibres showed the highest bond strength, while 3D** fibres showed the lowest bond strength. Also, the maximum uniaxial tensile stress for SFRLC specimens was determined while taking into consideration the random distribution of fibres in a practical situation.
- A fibre optimisation study was carried out, and it was concluded that incorporating multiple-bend fibres such as 5D fibres, which also have a high tensile strength of 2300 MPa, with a concrete of strength of 30 MPa can cause local fracturing of a lightweight concrete matrix. This is attributed to the difficulty of concrete to allow plastic hinge formation and straightening of the fibre during the pull-out process. Hence, it is advised that 5D fibres should not be employed as reinforcements for concrete of low grade. Also, 3D* and 4D fibres appeared to be the most efficient and optimum fibres for reinforcing lightweight concrete with tested strengths of 30–45 MPa, with the aspect ratio a_f playing a significant role in bond strength efficiency and the number of bends n_b having a greater impact on the energy dissipation efficiency.
- A semi-empirical constitutive tensile stress–crack width (σ-ω) model for fibrous lightweight concrete based on experimental testing was derived. The equations defining the residual tensile strengths $f_{lct,f1}$ and crack widths ω_{t1} were based on a regression analysis. The model showed its success in predicting the uniaxial tensile behaviour of SFRLC specimens. Since the model relies on the fibre reinforcing factor ρ_f (which is based on the fibre geometry and fibre volume fraction) and plain compressive or tensile strength, the model was also capable of validating the uniaxial tensile behaviour of steel-fibre-reinforced normal weight concrete from previous studies in the literature.
- The benefits of steel fibres in addressing the brittleness of lightweight concrete is of particular interest to designers and practitioners. This is in addition to the construction time savings from using fibres (which are simply added to the mix as opposed to steel laying). Using recycled-waste-based aggregates alongside fibres also adds to these practical benefits. The proposed constitutive model will allow designers to carry out more detailed analysis and design simulations in order to better understand the structural responses.
- In terms of future work, more research on SFRLC needs to be carried out at the structural level to include a comprehensive experimental testing programme of structural beams of different boundary and loading conditions, cross-sections, spans, and shear configurations. Numerical modelling can also be performed using the proposed material model. Some structural testing and finite-element analyses have been already undertaken, which will be reported in follow-up articles. The long-term behaviour of fibrous concrete remains largely unquantified by current standards, so this will benefit from further examination.

Author Contributions: Conceptualization, A.A.A.; methodology, A.A.A. and H.K.A.-N.; validation, H.K.A.-N.; formal analysis, H.K.A.-N.; investigation, A.A.A. and H.K.A.-N.; resources, A.A.A.; data curation, H.K.A.-N.; writing—original draft preparation, H.K.A.-N.; writing—review and editing, A.A.A.; visualization, H.K.A.-N.; supervision, A.A.A.; project administration, A.A.A. All authors have read and agreed to the published version of the manuscript.

Funding: This research received no external funding.

Data Availability Statement: The data presented in this study are available on request from the corresponding author due to technical/time limitations.

Conflicts of Interest: The authors declare no conflict of interest.

Notation

$f_{lck,cube}$	characteristic cube compressive stress
f_{lck}	characteristic cylinder compressive stress
f_{lc}	cylinder compressive stress
f_{lcm}	mean compressive cylinder stress
$f_{lcm,p}$	mean compressive cylinder stress of plain concrete
$f_{lcm,cube}$	mean cube compressive stress
$f_{lctm,m}$	maximum uniaxial tensile stress
A_f	area of a single fibre
d_f	fibre diameter
E_{lcm}	mean value of Young's modulus of elasticity
$E_{lcm,f}$	peak elastic modulus of SFRLC
n_b	number of bends
d_f	diameter of fibre
L_e	effective fibre anchorage length
L_E	embedded length of fibre
L_f	length of fibre
κ	fibre material factor
ρ_f	fibre reinforcing factor
δ	fibre shape factor
P_{max}	maximum pull-out strength for a single fibre
V_f	fibre volume fraction
W_p	total work performed by fibre
μ_{lc}	Poisson's ratio
ε	strain
ε_{lc1}	strain at peak compressive stress of LWAC
ε_{lcf}	strain at peak compressive stress of SFRLC
ε_{t1}	strain at post-cracking first residual tensile stress
ε_{lcu}	strain at ultimate compressive stress of LWAC
$\varepsilon_{lcf,ult}$	strain at ultimate compressive stress of SFRLC
η_0	fibre orientation factor
σ_f	fibre stress
τ_{av}	fibre–matrix interfacial bond shear stress
τ_{ult}	ultimate bond strength of SFRLC matrix
σ	stress
$\sigma_{av,f}$	average stress of fibre
σ_c	average stress of concrete
σ_y	fibre yield stress
σ_u	fibre ultimate stress
E_f	Young's modulus of elasticity fibre
SFRLC	steel-fibre-reinforced lightweight concrete
LWAC	lightweight aggregate concrete

References

1. Al-Khaiat, H.; Haque, M.N. Effect of initial curing on early strength and physical properties of lightweight concrete. *Cem. Concr. Res.* **1998**, *28*, 859–866. [CrossRef]
2. Gerritse, A. Design considerations for reinforced lightweight concrete. *Int. J. Cem. Compos. Lightweight Concr.* **1981**, *3*, 57–69. [CrossRef]
3. Lyag. *Technical Manual*; Lytag Ltd.: London, UK, 2011.
4. Lytag. Ramboll Frame Comparison Study. 2014. Available online: https://www.aggregate.com/our-businesses/lytag (accessed on 31 December 2019).
5. Chandra, S.; Berntsson, L. *Lightweight Aggregate Concrete Science*; Technology and Applications; Standard Publishers Distributors: Delhi, India, 2003; ISBN 81-8014-052-0.

6. Ahn, Y.B.; Jang, J.G.; Lee, H.K. Mechanical properties of lightweight concrete made with coal ashes after exposure to elevated temperatures. *Cem. Concr. Compos.* **2016**, *72*, 27–38. [CrossRef]
7. Libre, N.A.; Shekarchi, M.; Mahoutian, M.; Soroushian, P. Mechanical properties of hybrid fiber reinforced lightweight aggregate concrete made with natural pumice. *Constr. Build. Mater.* **2011**, *25*, 2458–2464. [CrossRef]
8. Campione, G. Flexural and Shear Resistance of Steel Fiber–Reinforced Lightweight Concrete Beams. *J. Struct. Eng.* **2014**, *140*, 04013103. [CrossRef]
9. Dias-da-Costa, D.; Carmo, R.N.F.; Graça-e-Costa, R.; Valença, J.; Alfaiate, J. Longitudinal reinforcement ratio in lightweight aggregate concrete beams. *Eng. Struct.* **2014**, *81*, 219–229. [CrossRef]
10. Mo, K.M.; Goh, S.; Alengaram, U.; Visintin, P.; Jumaat, M. Mechanical, toughness, bond and durability-related properties of lightweight concrete reinforced with steel fibres. *Mater. Struct.* **2017**, *50*, 46. [CrossRef]
11. Lim, W.; Mansur, K. Flexural behavior of reinforced lightweight aggregate concrete beams. In *Asia-Pacific Structural Engineering and Construction Conference*; APSEC: Kuala Lumpur, Malaysia, 2006; pp. 68–82.
12. Chen, H.; Huang, C.; Tang, C. Dynamic Properties of Lightweight Concrete Beams Made by Sedimentary Lightweight Aggregate. *J. Mater. Civ. Eng.* **2010**, *22*, 599–606. [CrossRef]
13. Wu, C.; Kan, Y.; Huang, C.; Yen, T.; Chen, L. Flexural behavior and size effect of full scale reinforced lightweight concrete beam. *J. Mar. Sci. Technol.* **2011**, *19*, 132–140. [CrossRef]
14. Badogiannis, E.; Kotsovos, M. Monotonic and cyclic flexural tests on lightweight aggregate concrete beams. *Earthq. Struct.* **2014**, *6*, 317–334. [CrossRef]
15. Lambert, G. Properties and Behaviour of Structural Lightweight (Lytag—Sand) Concrete. Ph.D. Thesis, University of Sheffield, Sheffield, UK, 1982.
16. Lo, T.Y.; Cui, H.; Memon, S.A.; Noguchi, T. Manufacturing of sintered lightweight aggregate using high-carbon fly ash and its effect on the mechanical properties and microstructure of concrete. *J. Clean. Prod.* **2016**, *112*, 753–762. [CrossRef]
17. Bilodeau, A.; Kodur, V.; Hoff, G. Optimization of the type and amount of polypropylene fibres for preventing the spalling of lightweight concrete subjected to hydrocarbon fire. *Cem. Concr. Compos.* **2004**, *26*, 163–174. [CrossRef]
18. Collins, R.; Sherwood, P. *Use of Waste and Recycled Materials as Aggregates*; H.M.S.O.: London, UK, 1995.
19. Gao, J.; Sun, W.; Morino, K. Mechanical properties of steel fiber-reinforced, high-strength, lightweight concrete. *Cem. Concr. Compos.* **1997**, *19*, 307–313. [CrossRef]
20. Campione, G.; La Mendola, L. Behavior in compression of lightweight fiber reinforced concrete confined with transverse steel reinforcement. *Cem. Concr. Compos.* **2004**, *26*, 645–656. [CrossRef]
21. Abbas, A.A.; Syed Mohsin, S.M.; Cotsovos, D.M. Seismic response of steel fibre reinforced concrete beam–column joints. *Eng. Struct.* **2014**, *59*, 261–283. [CrossRef]
22. Di Prisco, M.; Colombo, M.; Dozio, D. Fibre-reinforced concrete in fib Model Code 2010: Principles, models and test validation. *Struct. Concr.* **2013**, *14*, 342–361. [CrossRef]
23. Grabois, T.M.; Cordeiro, G.C.; Filho, R.D.T. Fresh and hardened-state properties of self-compacting lightweight concrete reinforced with steel fibers. *Constr. Build. Mater.* **2016**, *104*, 284–292. [CrossRef]
24. Abbas, A.A.; Syed Mohsin, S.M.; Cotsovos, D.M.; Ruiz-Teran, A.M. Shear behaviour of SFRC simply-supported beams, ICE Proc. *Struct. Build.* **2014**, *167*, 544–558. [CrossRef]
25. Ritchie, A.; Kayali, O. The effects of fiber reinforcement on lightweight aggregate concrete. In *Proceedings of RILEM Symposium on Fiber Reinforced Cement and Concrete*; Neville, A., Ed.; The Construction Press Ltd.: Hong Kong, China, 1975; pp. 247–256.
26. Swamy, N.; Jones, R.; Chiam, A. Influence of Steel fibers on the Shear Resistance of Lightweight Concrete I-Beams. *ACI Struct. J.* **1993**, *90*, 103–114.
27. Kang, T.; Kim, W. *Shear Strength of Steel Fiber-Reinforced Lightweight Concrete Beams*; Korea Concrete Institute: Oklahoma, TX, USA, 2010; pp. 1386–1392.
28. Iqbal, S.; Ali, A.; Holschemacher, K.; Bier, T. Mechanical properties of steel fiber reinforced high strength lightweight self-compacting concrete (SHLSCC). *Constr. Build. Mater.* **2015**, *98*, 325–333. [CrossRef]
29. IEA. *World Energy Outlook 2019*; IEA: Paris, France, 2019. Available online: https://www.iea.org/reports/world-energy-outlook-2019/coal#abstract (accessed on 1 October 2020).
30. Al-Naimi, H. Structural Behaviour of Steel Fibre Reinforced Lightweight Concrete. Ph.D. Thesis, Univeraity of East London, London, UK, 2020.
31. Al-Naimi, H.K.; Abbas, A.A. Constitutive model for plain and steel-fibre-reinforced lightweight concrete under compression. *Struct. Concr.* **2023**, *24*, 7625–7647. [CrossRef]
32. Kotsovos, M.D.; Pavlović, M.N. *Structural Concrete, Finite-Element Analysis for Limit-State Design*; Thomas Telford: London, UK, 1995.
33. Löfgren, I. Fibre-reinforced Concrete for Industrial Construction: A fracture mechanics approach to material testing and structural analysis. Ph.D. Thesis, Chalmers University Of Technology, Göteborg, Sweden, 2005.

34. Lee, S.-C.; Cho, J.-Y.; Vecchio, F.J. Diverse Embedment Model for Steel Fiber-Reinforced Concrete in Tension: Model Development. *ACI Mater. J.* **2011**, *108*, 516–525.
35. Kayali, O.; Haque, M.; Zhu, B. Some characteristics of high strength fiber reinforced lightweight aggregate concrete. *Cem. Concr. Compos.* **2003**, *25*, 207–213. [CrossRef]
36. Zhao, M.; Zhao, M.; Chen, M.; Li, J.; Law, D. An experimental study on strength and toughness of steel fiber reinforced expanded-shale lightweight concrete. *Constr. Build. Mater.* **2018**, *183*, 493–501. [CrossRef]
37. Badogiannis, E.G.; Christidis, K.I.; Tzanetatos, G.E. Evaluation of the mechanical behavior of pumice lightweight concrete reinforced with steel and polypropylene fibers. *Constr. Build. Mater.* **2019**, *196*, 443–456. [CrossRef]
38. Liu, X.; Wu, T.; Liu, Y. Stress-strain relationship for plain and fibre-reinforced lightweight aggregate concrete. *Constr. Build. Mater.* **2019**, *225*, 256–272. [CrossRef]
39. Mo, K.M.; Yap, K.K.Q.; Alengaram, U.J.; Jumaat, M.Z. The effect of steel fibres on the enhancement of flexural and compressive toughness and fracture characteristics of oil palm shell concrete. *Constr. Build. Mater.* **2014**, *55*, 20–28. [CrossRef]
40. *ASTM D638-10*; Standard Test Method for Tensile Properties of Plastics. ASTM International: West Conshohocken, PA, USA, 2014.
41. RILEM TC 162-TDF: Test and Design Methods for Steel Fibre Reinforced Concrete. Recommendations for uni-axial tension test. *Mater. Struct.* **2001**, *34*, 3–6. [CrossRef]
42. Abdallah, S.; Rees, D.W.A.; Hamidreza, S.; Fan, M. Understanding the effects of hooked-end steel fibre geometry on the uniaxial tensile behaviour of self-compacting concrete. *Constr. Build. Mater.* **2018**, *178*, 484–494. [CrossRef]
43. Abdallah, S.; Fan, M.; Zhou, X. Effect of Hooked-End Steel Fibres Geometry on Pull-Out Behaviour of Ultra-High Performance Concrete. *Int. J. Civ. Environ. Struct. Constr. Archit. Eng.* **2016**, *10*, 1594–1599.
44. Bekaert. 2020. Available online: https://www.bekaert.com/en/ (accessed on 20 June 2020).
45. Robins, P.; Austin, S.; Jones, P. Pull-out Behaviour of Hooked Steel Fibres. *Mater. Struct.* **2002**, *35*, 434–442. [CrossRef]
46. Alwan, J.; Naaman, A.; Guerrero, P. Effect of mechanical clamping on the pull-out response of hooked steel fibers embedded in cementitious matrices. *Concr. Sci. Eng.* **1999**, *1*, 15–25.
47. Abdallah, S.; Fan, M.; Rees, D.W.A. Analysis and modelling of mechanical anchorage of 4D/5D hooked end steel fibres. *Mater. Des.* **2016**, *112*, 539–552. [CrossRef]
48. Abdallah, S.; Fan, M.; Zhou, X. Pull-Out Behaviour of Hooked End Steel Fibres Embedded in Ultra-high Performance Mortar with Various W/B Ratios. *Int. J. Concr. Struct. Mater.* **2017**, *11*, 301–313. [CrossRef]
49. Romualdi, J.P.; Mandel, J.A. Tensile Strength of Concrete Affected by Uniformly Distributed and Closely Spaced Short Length of Wire Reinforcement. *ACI J. Proc.* **1964**, *61*, 657–671.
50. Krenchel, H. Fibre Spacing and Specific Fibre Surface. In *Testing and Test Methods of Fibre Cement Composites*; Proceedings of the RILEM Symposium; Construction Press Ltd.: Lancaster, UK, 1978; pp. 69–79.
51. Soroushian, P.; Lee, C.-D. Tensile Strength of Steel Fiber Reinforced Concrete: Correlation with Some Measures of Fiber Spacing. *ACI Mater. J.* **1990**, *87*, 541–546.
52. Wille, K.; Naaman, A.E. Pullout behavior of highstrength steel fibers embedded in ultra-high-performance concrete. *ACI Mater. J.* **2012**, *109*, 479–588.
53. Wille, K.; Naaman, A.E. Effect of ultra-high-performance concrete on pullout behavior of high-strength brass-coated straight steel fibers. *ACI Mater. J.* **2013**, *110*, 451–462.
54. Cao, Y.Y.Y.; Yu, Q.L. Effect on inclination angle on hooked end steel fiber pull out behavior in ultra-high performance concrete. *Compos. Struct.* **2018**, *201*, 151–160. [CrossRef]
55. Qi, J.; Wu, Z.; Ma, Z.J.; Wang, J. Pullout behaviour of straight and hooked-end steel fibers in UHPC matrix with various embedded angles. *Constr. Build. Mater.* **2018**, *191*, 764–774. [CrossRef]
56. Barragán, B.E.; Gettu, R.; Martín, M.A.; Zerbino, R.L. Uniaxial tension test for steel fibre reinforced concrete—-A parametric study. *Cem. Concr. Compos* **2003**, *25*, 767–777. [CrossRef]
57. Abdallah, S.; Rees, D.W.A. Comparisons Between Pull-Out Behaviour of Various Hooked-End Fibres in Normal–High Strength Concretes. *Int. J. Concr. Struct. Mater.* **2019**, *13*, 27. [CrossRef]
58. Lim, T.Y.; Paramasivam, P.; Lee, S.L. Analytical Model for Tensile Behaviour of Steel-Fibre Concrete. *ACI Mater. J. Tech. Pap.* **1987**, *84*, 286–298.
59. Lok, T.; Xiao, J. Tensile behaviour and moment–curvature relationship of steel fibre reinforced concrete. *Mag. Concr. Res.* **1998**, *50*, 359–368. [CrossRef]
60. Lok, T.-S.; Xiao, J.R. Flexural Strength Assessment of Steel Fiber Reinforced Concrete. *J. Mater. Civ. Eng.* **1999**, *11*, 188–196. [CrossRef]
61. Hannant, D.J. *Fibre Cements and Fibre Concrètes*; John Wiley & Sons, Ltd.: Hoboken, NJ, USA, 1978.
62. Joo Kim, D. *Strain Rate Effect on High Performance Fiber Reinforced Cementitious Composites Using Slip Hardening High Strength Deformed Steel Fibers*; University of Michigan: Ann Arbor, MI, USA, 2009.

63. Naaman, A.E.; Namur, G.G.; Alwan, J.M.; Najm, H. Fiber pull-out and bond slip, Part I: Analytical study. *ASCE J. Struct. Eng.* **1991**, *117*, 2769–2790. [CrossRef]
64. De Montaignac, R.; Massicotte, B.; Charron, J.-P.; Nour, A. Design of SFRC structural elements: Post-cracking tensile strength measurement. *Mater. Struct.* **2011**, *45*, 609–622. [CrossRef]
65. Fédération Internationale du béton. *fib Model Code for Concrete Structures 2010*; Ernst and Sohn: Berlin, Germany, 2013; pp. 147–150.
66. *BS EN 1992:1:1*; Eurocode 2: Design of Concrete Structures—Part 1: General Rules and Rules for Buildings. Comité Européen De Normalisation: Bruxelles, Belgium, 2004.